Cystatin M/E ameliorates bone resorption through increasing osteoclastic cell estrogen influx

Jin-Ran Chen

chenjinran@uams.edu

University of Arkansas for Medical Sciences https://orcid.org/0000-0001-6984-5878

Dongzheng Gai

University of Arkansas for Medical Sciences

Perry Caviness

UAMS

Oxana Lazarenko

UAMS

Jennifer Chen

University of Arkansas

Christopher Randolph

UAMS

Zijun Zhang

UAMS

Yan Cheng

UAMS

Fumou Sun

UAMS

Hongwei Xu

UAMS

Michael Blackburn

UAMS

Guido Tricot

UAMS

John Shaughnessy Jr

UAMS

Fenghuang Zhan

UAMS

Article

Keywords:

Posted Date: May 6th, 2024

DOI: https://doi.org/10.21203/rs.3.rs-4313179/v1

Additional Declarations: (Not answered)

Cystatin M/E ameliorates bone resorption through increasing osteoclastic cell estrogen influx

Dongzheng Gai[1, 2*], Perry C. Caviness[3, 4*], Oxana P. Lazarenko[3, 4], Jennifer F. Chen[5], Christopher E. Randolph[6], Zijun Zhang[1], Yan Cheng[1], Fumou Sun[1], Hongwei Xu[1], Michael L Blackburn[3, 4], Guido Tricot[1], John D Shaughnessy Jr[1], Jin-Ran Chen[3, 4#], Fenghuang Zhan[1#]

Affiliations:

[1]Myeloma Center, Winthrop P. Rockefeller Cancer Institute, Department of Internal Medicine, University of Arkansas for Medical Sciences, Little Rock, Arkansas, USA.

[2]Department of Hematology, Heping Hospital Affiliated to Changzhi Medical College, Changzhi, Shanxi, 046000, China.

[3]Arkansas Children's Nutrition Center, Little Rock, AR 72205, USA.

[4]Department of Pediatrics, University of Arkansas for Medical Sciences, Little Rock, AR 72205, USA.

[5]Undergraduate Pre-Medical Program, University of Arkansas at Fayetteville, Fayetteville, AR, 72701, USA.

[6]Center for Translational Pediatric Research, Arkansas Children's Research Institute, Little Rock, AR 72202, USA.

* These authors contributed equally to this work; # These authors are equal senior and corresponding authors.

Corresponding Authors: Fenghuang Zhan and Jin-Ran Chen, Myeloma Center, Winthrop P. Rockefeller Cancer Institute, Department of Internal Medicine, University of Arkansas for Medical Sciences, 4301 W. Markham St. Slot# 508, Little Rock, AR, USA 72205. Tel: 501-526-6000 ext. 25228. E-mail: FZhan@uams.edu or Chenjinran@uams.edu. Arkansas Children's Nutrition Center, Department of Pediatrics, University of Arkansas for Medical Sciences, Little Rock, AR 72205, USA.

Abstract

In multiple myeloma (MM), increased osteoclast differentiation leads to the formation of osteolytic lesions in most MM patients. Bisphosphonates, such as zoledronic acid (ZA), are used to ameliorate bone resorption, but due to risk of serious side effects as well as the lack of repair of existing lesions, novel anti-bone resorption agents are required. Previously, the absence of osteolytic lesions in MM was strongly associated with elevated levels of cystatin M/E (CST6), a cysteine protease inhibitor, secreted by MM cells. In this study, both MM- and ovariectomy (OVX)-induced osteoporotic mouse models were used to compare the effects of recombinant mouse CST6 (rmCst6) and ZA on preventing bone loss. μCT showed that rmCst6 and ZA had similar effects on improving percent bone volume, and inhibited differentiation of non-adherent bone marrow cells into mature osteoclasts. Single-cell RNA sequencing showed that rmCst6 and not ZA treatment reduced bone marrow macrophage percentage in the MM mouse model compared to controls. Protein and mRNA arrays showed that both rmCst6 and ZA significantly inhibit OVX-induced expression of inflammatory cytokines. For OVX mice, ERα protein expression in bone was brought to sham surgery level by only rmCst6 treatments. rmCst6 significantly increased mRNA and protein levels of ERα and significantly increased total intracellular estrogen concentrations for *ex vivo* osteoclast precursor cell cultures. Based on these results, we conclude that CST6 improves MM or OVX bone loss models by increasing the expression of estrogen receptors as well as the intracellular estrogen concentration in osteoclast precursors, inhibiting their maturation.

Significance

Recombinant mouse CST6 shows bone protective abilities for both multiple myeloma and ovariectomy mouse models through increasing osteoclastic cell estrogen influx.

Introduction

Multiple myeloma (MM) is a malignancy of terminally differentiated B-cells that is localized primarily in the bone marrow (BM) but also can be present in peripheral blood and tissue/organs. MM cells expand in the BM, produce extra and abnormal proteins and may crowd out healthy BM cells suppressing BM function[1]. MM symptoms include hypercalcemia, anemia, renal insufficiency, and osteolysis. Osteolysis, a hallmark of MM, is the cause of severe complications seen in nearly 80% of MM cases and is the result of interactions between MM cells and the BM microenvironment leading to increased osteoclast differentiation and suppressed osteoblast differentiation, resulting in increased bone resorption and the presence of osteolytic bone lesions[2,3]. These lesions frequently cause bone pain and lead to complications, including pathological fractures, vertebral collapse, spinal cord compression, hypercalcemia, and generalized osteoporosis, compromising MM patient quality of life, impairing survival odds, and increasing treatment costs for MM patients[4].

Bisphosphonates (BPs) are extensively utilized in clinical practice for the treatment of diseases associated with high bone resorption, such as osteoporosis, Paget's disease, and cancer-induced bone disease[5-7]. BPs are pyrophosphate analogs that bind to exposed bone areas of hydroxyapatite crystals[8]. During bone remodeling, they are absorbed by osteoclasts, and through inhibition of intracellular farnesyl pyrophosphate synthase as well as the suppression of GTPase prenylation and interference with downstream pathways, BPs suppress formation of osteoclasts from precursors and induce apoptosis of mature osteoclasts[9,10.]

Based on their chemical structure, BPs are divided into two main groups: nitrogen and non-nitrogen containing[5]. Among BPs, zoledronic acid (ZA) is the most extensively used in treating cancer-induced bone disease[11]. In subsets of MM patients, clinical trials showed that ZA combined with other novel anti-MM agents reduced skeletal related events (SREs), prolonged the period between remission and recurrence, and improved the overall survival[12,13]. However, although ZA and other anti-resorption drugs are effective at inhibiting osteoclastic bone resorption, the inability of these compounds to repair existing osteolytic lesions and the potential adverse side effects associated with long-term use of such anti-bone resorption drugs, including renal impairment and osteonecrosis of jaw (ONJ), necessitate the development of novel agents[3,14,15].

Other anti-resorption drugs, like the RANKL monoclonal antibody Denosumab were approved by the FDA to treat MM bone disease; however, the same adverse effects seen with ZA are also found in treated patients with Denosumab[15]. Recently, we combined PET-CT scanning with global gene expression profiling of BM CD138-selected plasma cells (PC) from 512 newly diagnosed MM patients to show that the absence of osteolytic lesions is linked to elevated expression of cystatin M/E (CST6), a cysteine protease inhibitor, secreted by MM cells. Recombinant CST6 protein inhibits the activity of the osteoclast-specific protease cathepsin K, blocks osteoclast differentiation and function, and inhibits bone destruction *in ex vivo* and *in vivo* myeloma models. Suppression of cathepsin L blocks cleavage of p100 to p52 as well as degradation of TRAF3, suppressing the alternative NF-κB pathway[16]. Furthermore, Li et al. reported that CST6 and CST6 peptides (containing the conserved QLVAG residues) inhibit breast cancer bone metastasis by suppressing cathepsin B activity[17].

In our current study, we utilized both MM- and ovariectomy (OVX)-induced osteoporosis mouse models to compare the effects of ZA and recombinant mouse CST6 (rmCst6) on bone resorption. Single-cell RNA-seq was used to show BM cell populations in murine MM mice following treatment with either rmCst6 or ZA. Previously, it was shown that in breast cancer, loss of CST6 led to a subsequent loss of estrogen receptor alpha (*ERα)*[18]. Estrogen is an important regulator of bone turnover, decreasing the rate of bone resorption and increasing the rate of bone formation, and its actions on bone cells are carried out through interactions with estrogen receptors such as ERα and ERβ. We thus decided to investigate CST6 effect on intracellular estrogen concentration in osteoclast precursors on protecting against bone deterioration in both MM osteolytic bone disease mouse models and OVX mouse models. The effect of CST6 on estrogen transport and estrogen related genes in bone tissue as well as osteoclast precursors were also investigated. It is our hope that this research will assist in the development of novel bone anti-resorption drugs for the treatment of MM osteolytic lesions as well as for other bone resorption disorders such as osteoporosis.

Results

Evaluate rmCst6 protein and ZA inhibition in MM cell-induced bone resorption *in vivo*

The 5TGM1-KaLwRij murine MM model was utilized to compare the effect of CST6 protein and ZA *in vivo* on treating MM induced bone disease. One million 5TGM1 cells were inoculated into C57BL/KaLwRij mice via the tail vein and mice were treated with purified

rmCst6, ZA or PBS (**Figure 1A**). Intravenous (i.v) injection of purified rmCst6 protein (200 μg/kg, twice per week) and subcutaneous (s.c) injection of ZA (100 μg/kg, twice per week) improved bone compared to PBS injection, while also significantly decreasing the number of osteolytic lesions in MM-bearing mice (**Figure 1B and 1C**). μCT reconstruction of mouse tibia showed that rmCst6 protein and ZA significantly increased trabecular bone volume over total volume (BV/TV), trabecular number (Tb.N) and bone mineral density (BMD). However, rmCst6 or ZA treatment of MM mouse models had no significant effect on trabecular thickness (Tb. Th) or trabecular separation (Tb. Sp) (**Figure 1B and 1C**). Additional data for MM mouse model μCT results are listed in **Table 1**. Histomorphometric analyses demonstrated that rmCst6 and ZA administration significantly reduced osteoclast (OC) numbers as well as the proportion of bone surface occupied by osteoclasts in MM-bearing mice (**Figure 1D and 1E**). ZA treatment caused the appearance of bone to be somewhat osteopetrotic when compared to rmCst6 (**Figure 1B**). To determine whether CST6 or ZA influenced MM tumor burden, flow cytometry was performed to detect the bone marrow GFP+5TGM1 cells in the tibiae at the time of sacrifice. There was no difference between MM bearing mice and MM mice treated with rmCst6 or ZA (**Figure 1F and 1G**). Furthermore, ELISA measurements of tumor-specific M protein, IgG2b, in serum from MM-bearing mice with or without rmCst6 and ZA therapy after 25 days revealed no difference between the control and either treatment group (**Figure 1H**). Finally, ELISA analyses showed that levels of the C-terminal telopeptide of type-I collagen (CTX-1), which is a biomarker of the rate of bone turnover and osteoclast activity, were significantly reduced in mice treated with ZA and rmCst6 (**Figure 1I**).

Evaluate rmCst6 protein and ZA effects in an ovariectomized (OVX) mouse model

We next determined if CST6 could inhibit bone loss in a murine model of estrogen deprivation-induced osteoporosis similar to ZA. Six-month old C57/BL6 ovariectomized (OVX) mice were treated with PBS, ZA or rmCst6 for 6 weeks (**Figure 2A**). After 6 weeks, mice were sacrificed and tibias were analyzed by μCT and histology. Compared with the sham group, tibias from the OVX mice exhibited significant bone loss, and treatment with either rmCst6 or ZA appeared to improve bone quality back to sham surgery levels or better (**Figure 2B and 2C**). Quantitative analysis confirmed that bone parameters, including BV/TV, Tb.N, and BMD improved in the OVX + rmCst6 mice compared to OVX mice. BV/TV, Tb. N, Tb.Sp, and BMD bone parameters improved in OVX + ZA mice compared to just OVX mice. Tb.Th was not

improved in OVX mice after treatment with ZA or rmCst6 (**Figure 2C**). Similar to the MM mouse model, μCT demonstrated that a thick band of calcified trabeculae with distorted architecture somewhat osteopetrotic under the growth plate in OVX mice treated after ZA (**Figure 2B**). Data for OVX mouse model μCT results are listed in **Table 2**. Histomorphometric analyses demonstrated that rmCst6 administration significantly reduced the number of TRAPase positive cells in OVX mice. However, after 6 weeks of ZA treatment, quantitative statistical histomorphometry showed a significant increase in TRAPase positive cells in the trabecular bone region, especially on the surface of calcified cartilage that fills the tibia metaphysis (**Figure 2D and 2E**). The number of adipocyte-like cells in the tibia metaphysis was also measured; there was an initial rise after OVX that was reduced to sham levels after treatment with rmCst6 and to below sham levels after treatment with ZA (**Figure 2F**). Finally, ELISA analysis showed that CTX-1 and P1NP levels were significantly reduced in mice treated with ZA and rmCst6 protein following OVX compared to OVX mice alone (**Figure 2G and 2H**).

Cell composition of MM mouse bone marrow is altered by rmCst6 and ZA treatment

Single cell RNA sequencing (scRNA-seq) was used to examine the effect of ZA and rmCst6 on the bone marrow (BM) cell composition in MM mouse models (**Figure 3A**). Based on expression key genes cells were sorted into specific categories. Uniform Manifold Approximation and Projection (UMAP) plot of BM mononuclear cells indicated that MM cells induced an increase in the percentage of monocyte progenitors and a decrease of B cell percentage in BM (**Figure 3B and 3C**). When compared to other groups, only rmCst6 treated mice showed a decrease in BM macrophage percentage and an increase in BM monocyte percentage (**Figure 3B and 3C**). ZA treated mice alone showed an increase in BM mature neutrophil percentage (**Figure 3B**).

Since it is known that macrophages are osteoclast precursors, the change in percentage of previously identified macrophage subtypes was also investigated using UMAP plots of BM macrophages following MM mouse treatment with either PBS, rmCst6 or ZA[16]. rmCst6 and ZA treatment was found to decrease percentage of M0 and M4 macrophages, identified as early precursors of osteoclasts and tumor associated macrophages with high expression of osteoclast differentiation regulators (*Jun* and *c-Fos*)[16,19]. rmCst6 and ZA also decreased the percentage of M5 macrophages, while ZA alone decreased percentage of M3 macrophages (**Supplemental Figure 1**). rmCst6 treatment was unexpectedly shown to increase percentage of M7

macrophages while ZA treatment also increased percentage of M2 macrophages. M3 macrophages produce inflammatory cytokines and are thought to have tumor suppressing abilities[20]. M1, M2, M5 and M7 macrophages were classified as being involved in neurological disorders and viral infections but not osteoclastogenesis[16].

Effects of rmCST6 and ZA on the viability and differentiation of osteoclasts, osteoblasts and chondrocytes

rmCst6 has previously been shown to suppress MM induced osteolytic bone disease through interfering with osteoclast differentiation and function but not viability[16]. On the other hand, ZA was shown to suppress skeletal related events in MM induced osteolytic bone disease through inactivation and apoptosis of osteoclasts[1]. To compare the effects of rmCst6 and ZA on suppressing osteoclastogenesis, mouse BM monocytes were induced to differentiate into osteoclasts by addition of M-CSF (10 ng/ml) and RANKL (10 ng/ml) in the presence or absence of rmCst6 or ZA. TRAPase staining showed that rmCst6 and ZA significantly suppressed the formation of TRAPase-positive multinuclear osteoclasts in a dose-dependent manner (**Figure 4A**). However, different from rmCst6, ZA appears to be more effective at promoting cell death, as no cells (osteoclasts or precursors) are present at 5 μM ZA (**Figure 4A and 4B**). Perhaps the ZA specific effects on osteoclastic cells might explain ZA-related osteonecrosis.

While ZA was shown to effectively suppress osteoclastogenesis through cell death there is controversial evidence suggesting ZA can impact osteoblast function[5,10]. To evaluate the effects of rmCst6 and ZA on osteoblast cell viability and differentiation, mouse osteoblast progenitor MC3T3-E1 cells were exposed to different doses of ZA and 200 ng/ml rmCst6, the most effective dose for preventing osteoclast differentiation. Alkaline phosphase (ALP), a relative early marker of osteoblast differentiation, staining was performed to assess the effects of ZA and CST6 on the MC3T3-E1 differentiation. Following 14 days treatment, ALP staining showed that ZA, but not CST6, significantly suppress the osteoblast differentiation (**Figure 4C**). The mineralization capacity of cultured osteoblasts treated with ZA and rmCst6 for 21 days were also evaluated using Alizarin Red assay. Again, ZA but not rmCst6, significantly inhibited the formation of mineralized nodules in a dose-dependent manner (**Figure 4C**). Because of the effect of ZA on pre-osteoblast differentiation and mineralization, cell viability of MC3T3-E1 cells treated with increasing concentrations of ZA was analyzed. CCK-8 cell viability assay showed that ZA had a significant dose-dependent decrease in cell viability starting at 1 μM (**Figure 4D**).

This data suggests that compared with rmCst6, ZA decreased the osteoblast activity and function.

In addition to osteoblastogenesis, endochondrogenesis is also critical for bone formation. To assess the effect of rmCst6 or ZA on chondrogenesis, teratocarcinoma stem cell line ATDC5 was utilized to determine the effect of both treatments on pre-chondrocyte differentiation, mineralization, and cell viability[21]. Following 14 days of treatment in chondrocyte differentiation medium, alcian blue staining demonstrated that the glycosaminoglycan (GAG)-rich extracellular matrix (ECM) found during chondrogenesis was suppressed by ZA treatment but not rmCst6 (**Figure 4E**). ATDC5 cells can mineralize surrounding ECM to produce mineral nodules. As such, alizarin red staining was performed and it was shown that ZA treatment and not rmCst6 inhibited ATDC5 mineralization (**Figure 4E**). Finally, CCK-8 cell viability assay showed that, similar to osteoblast precursors starting at 2 μM ZA, ATDC5 cell viability was significantly decreased in a dose-dependent manner (**Figure 4F**).

rmCst6 and ZA bring OVX induced inflammatory cytokine levels back to control

Inflammation is a key factor in osteoclastogenesis, as such the anti-inflammatory effects (and thus the anti-bone resorptive effects) of the treatments used in this study (rmCst6 and ZA) as well as the proinflammatory effects of OVX were measured using an inflammatory cytokine array Raybiotech. The 25 targets with the largest initial change in membrane intensity from the Sham surgery group to the OVX-PBS group are shown (**Figure 5**). The anti-inflammatory effects of rmCst6 and ZA appear to be equivalent. Data and statistics for 25 targets with the largest initial change in membrane intensity following OVX are listed in **Table 3**. The complete data set for inflammatory cytokine array is listed in supplemental file 1.

ZA and rmCst6 treatment upregulate different genomic pathways in bone of OVX mice

For the OVX model it was shown that both rmCst6 and ZA ameliorated OVX induced inflammation (and thus potentially bone resorption) back to sham surgery levels. To determine the mechanisms by which rmCst6 and ZA suppress bone resorption, sequencing analysis of RNA isolated from the tibia of OVX mice treated with either rmCst6 or ZA was performed (**Figure 6A**). Between the OVX-PBS and the OVX-rmCst6 treatment groups, there were 175 differentially expressed genes unique to the rmCst6 treatment; between the OVX-PBS and the OVX-ZA treatment groups, there were 12 differentially expressed genes unique to the ZA treatment and there are 3 differentially expressed genes shared between both OVX-PBS vs

OVX-rmCst6 and OVX-PBS vs OVX-ZA (**Figure 6B**). The 10 genes with the largest fold compared to OVX-PBS are listed for both the rmCst6 and ZA treatment (**Figure 6C and 6D**). Of particular interest, for rmCst6 treatment, the solute carrier organic anion transporter family member 1a4 (*Slco1a4*), an organic anion transporter, had the largest fold increase (log2 fold = 3.60), while for ZA treatment, *MMP9*, which plays a role in apoptotic pathways, had the greatest fold increase (log2 fold = 3.33)[22,23]. Since ZA, is known for apoptotic effects on bone cells, the effect of rmCst6 on *Slco1a4* gene expression was investigated further. Basal *Slco1a4* RNA levels were found for different bone tissues and cells using PCR and agarose gel electrophoresis (Tissue: tibia, vertebrae, isolated bone marrow cells and empty femur; Cell types: Raw 264.7, ST2, OB6, ATDC5 and MLOY4) (**Figure 6E and 6F**). Real-time PCR for RNA isolated from OVX mice L3-L5 vertebrae matched RNA-seq results, mRNA levels were decreased following OVX and only rmCst6 treatment brought *Slco1a4* mRNA back to sham surgery levels (**Figure 6G**). To determine cell types where rmCst6 treatment increases Slco1a4 gene expression real-time PCR was performed for macrophage Raw 264.7 cells (+/- 20 ng/ml RANKL) and stromal ST2 cells (+/- 1 mM A2P). For Raw 264.7 cells, only rmCst6 (+ 20 ng/ml RANKL) displayed a dose dependent increase in *Slco1a4* mRNA levels up to 100 ng/ml rmCst6 (**Figure 6H**). rmCst6 treatment also increased Slco1a4 mRNA levels in osteoblast precursor ST2 cells (+/- 1 mM A2P), however based on one-way ANOVA changes were not considered significant (Figure 6I and 6J). Normalized, log(2) gene expression for RNA-seq data is listed in supplemental file 2.

rmCst6 treatment increases intracellular estrogen concentration of osteoclast precursors

Due to structural and sequence similarities in the solute carrier organic anion transporter family, *Slco1a4* is predicted to play a role in Na^+ independent transport of estrogen and its derivatives across the plasma membrane into the cell[24-26]. Previously it was found that loss of CST6 in breast cancer led to a loss of ERα expression[18]. As such, we investigated the effect of rmCst6 treatment on estrogen transport and its downstream effects. Protein expression of ERα in L3-L5 was investigated for mice subject to sham surgery or OVX and treated with ZA or rmCst6. When compared to sham surgery mice, ERα protein levels are decreased for OVX mice and brought back to near sham levels only by treatment with rmCst6 but not ZA (**Figure 7A**). ERα mRNA and protein levels were analyzed at the cellular level using Raw 264.7 cells (+/- 20 ng/ml RANKL). For Raw 264.7 cells incubated in the presence and absence of RANKL, treatment with rmCst6 significantly increased ERα mRNA levels compared to control. For Raw

264.7 cells incubated in the absence of RANKL, 1 μM ZA also increased ERα mRNA levels. ERα protein levels were also increased for Raw 264.7 cells (+/- 20 ng/ml RANKL) (**Figure 7B and 7C**). Protein band intensity data quantified by imageJ and normalized to β-actin intensity are listed in **Table 4** and **Table 5**.

Total intracellular estrogen (Estrone; E1, 17-β-estradiol; E2 or Estriol; E3) concentration was evaluated in non-adherent mouse bone marrow cells (pre-osteoclasts) isolated from the femur following 72 hr. treatment with either ZA or 100 ng/ml rmCST6. Intracellular total estrogen concentration was significantly increased following treatment with 100 ng/ml rmCst6. Treatment with ZA did not significantly alter intracellular estrogen concentration compared to control (**Figure 7D**). Immunohistochemistry was used to investigate alterations in estrogen responsive genes in Raw 264.7 cells treated with 100 ng/ml rmCST6. At 24 hr. incubation, ERα expression was increased following rmCst6 treatment. PPARγ expression, which is suppressed by estrogen, was lowered following rmCst6 treatment (**Figure 7E**). Raw 264.7 cells were incubated for 7 days with 20 ng/ml RANKL to determine the rmCst6 affects the expression of estrogen responsive genes in macrophage-like cells differentiating into osteoclasts. Similar to the 24 hr. incubation period, treatment with 100 ng/ml rmCst6 caused an increase in the expression of ERα and a decrease in the expression of PPARγ (**Figure 7F**). We validated the remarkable influx of estrogen into Raw 264.7 cells after treatment with 100 ng/ml rmCst6 for 24 hours (**Figure 7G**).

Discussion

In this study, we show that rmCst6 treatment recovers bone mass in both MM and OVX mouse models without the increased trabecular thickness comparable to the commonly prescribed bisphosphonate ZA. rmCst6 was shown to be as effective as ZA at suppressing osteoclast cell proliferation and viability without cytotoxic effects towards osteoblast and chondrocyte cell lines. When compared to ZA, rmCst6 was shown to significantly increase intracellular estrogen concentration in mouse bone marrow cells. In both male and female bone, estrogen plays an important role in regulating bone turnover, impacting both osteoclast and osteoblast function through a variety of different pathways[27-30]. As such, biomolecules with the ability to regulate estrogen influx in bone cells would be highly prized as novel agents for combating diseases associated with increased bone resorption.

Based on UMAP results for MM mice, estrogen may attenuate monocyte polarization into macrophage cell type through suppressing expression of key inflammatory factors, explaining the rmCst6 induced increase in monocyte cells and decrease in macrophages[16,31–33]. A depletion in macrophage cell percentage would in turn lead to a depletion in osteoclasts and thus suppression of bone resorption. Both rmCst6 and ZA treatments were also shown to affect the different macrophage subtypes present in the bone marrow. M0, M4 and M5 macrophage subtypes were significantly decreased in both rmCst6 and ZA treated MM mouse models. M0 macrophages are undifferentiated macrophages with potential to polarize into different macrophage sub-types, including osteoclasts[19]. The specific role of M4 macrophages is currently unknown, however this subtype has previously been shown to have increased expression of osteoclast differentiation genes[16]. As with the decrease in total BM macrophage cell percentage the decrease in M0 and M4 macrophage subtypes following rmCst6 treatment can potentially be explained as estrogen preventing monocyte polarization to macrophage cell types and macrophage polarization into osteoclasts[16,31-34]. For ZA treatment, decrease in M0 and M4 macrophages may be from known apoptotic effects of ZA[22]. In the context of MM osteolysis as well as other bone resorption disorders, suppression of macrophage cell percentage, as well as a decrease in M0 and M4 macrophage subtypes would explain the bone protective effects of both rmCst6 and ZA.

Currently the decrease in M5 and M3 macrophage following ZA treatment can be explained in the context of MM. For ZA, apoptosis may again explain the decrease M5 and M3 macrophages. Potential apoptosis of anti-tumor acting M3 macrophages hint that ZA alone may not be most effective at treating MM osteolytic bone disease[20,22]. For rmCst6 treatment suppression of M5 macrophages and increased expression of M7 macrophages are more difficult to explain. As M5 and M7 macrophages are thought to play a role in the immune system, Cst6 may impact M5 and M7 macrophage levels through inhibition of key cysteine proteases involved in immune system regulation[35]. However, will be needed to clarify the precise mechanism explaining rmCst6 induced increase in M5 and M7 macrophages. M2 macrophage involvement in oxidative stress repair pathways may explain their increase following ZA treatment due to increased ROS[22,36].

To further investigate the ability of rmCst6 as an inhibitor of bone resorption, rmCst6's impact on osteoclastogensis on mouse primary non-adherent BM cells was compared to ZA.

rmCst6 was found to have a dose dependent effect on osteoclast number while ZA, even at low concentrations significantly depleted number of osteoclast and precursor cells. In addition to osteoclasts, ZA was also found to have significant suppressive effects on cell vitality of osteoblast (MC3T3-E1) and chondrocyte (ATDC5) precursors hinting towards toxicity from long term ZA use[37,38]. In contrast to ZA, rmCst6 at the highest concentration available (200 ng/ml) had no cytotoxic effects on osteoblast and chondrocyte cell vitality, further hinting towards its potential as an alternative to ZA. However, the efficacy, bioavailability and long-term safety of rmCst6 compared to ZA will need to be addressed in future studies.

In the OVX model, both rmCst6 and ZA were shown to decrease OVX induced increase in inflammatory cytokines back to sham surgery levels. While inflammatory cytokine array was performed for only OVX model, in the context of sex steroid deficiency as well as MM induced bone loss, suppression of inflammatory factors would suppress osteoclastogenesis and thus bone resorption. Sex steroid deficiency is known to cause an increase in adipocyte-like cells present in the bone marrow, explaining increase in adipocyte like cells from OVX mouse model histology results. This increase in adipose tissue would in turn cause an increase in inflammatory factors and thus bone resorption[39]. CST6's ability to promote estrogen efflux may explain this decrease in adipose tissue[40]. In addition, estrogen has been shown to suppress expression of inflammatory cytokines such as TNFα, BLC (CXCL13) and SCF[41-43]. ZA was also shown to suppress adipocyte-like cell formation and expression inflammatory factors. In the context of the OVX model, ZA induced effect on inflammatory factors may also be through suppression of adipose tissue formation. Currently the mechanism by which ZA reduces adipogenesis is unknown. However, based on previous results for osteoblast and chondrocyte cell lines, high concentrations of ZA may also promote apoptosis of adipocyte-like cells[22]. ZA was also shown to significantly increase the number of TRAP positive cells in BM of OVX mice tibia. Increased number of TRAP positive cells and mRNA levels of *MMP9* may be due to ZA causing an increase in the number of "non-attached" osteoclasts undergoing prolonged apoptosis[22,44,45]. In the future the impact of rmCst6 as well as ZA on the expression of inflammatory cytokines in MM mice will need be studied.

The mechanism by which rmCst6 promotes estrogen influx in macrophage precursors is currently unknown. Based on OVX model RNA-seq data, expression of the organic anion transport protein *Slco1a4* is increased following treatment with rmCst6. In humans, the *Slco1a4*

gene analog includes both estrone-3-sulfate and 17β-estradiol-glucuronide as substrates[24-26]. While the OVX mouse model is "sex steroid deficient" it has been shown that levels of estrone (E1), are higher in post-menopausal women, potentially explaining the bone protective ability of rmCst6 in this model[46]. Based on real-time PCR results from cell lines, upregulation of *Slco1a4* following rmCst6 treatment may partially explain the increase in intracellular estrogen concentration in bone marrow primary cell lines. While Raw 264.7 and ST2 cell lines can differentiate into mature osteoclasts and osteoblasts, respectively, they are not primary precursor cells, and as such, the expression of Slco1a4 will need to be determined in primary osteoclast or osteoblast precursor cells isolated from bone marrow. It will also need to be determined if Slco1a4 is upregulated in MM mice following rmCst6 treatment. To establish *Slco1a4* as a factor in rmCst6 induced estrogen influx, further research is needed.

Cystatins are not thought to make the cell membrane more permeable to biomolecules such as estrogen. To explain the increase in intracellular estrogen levels in osteoclast precursors following rmCst6 treatment, estrogen transport would need to be increased from upregulated expression of plasma membrane localized ERα (and potentially Slco1a4). However, a mechanism explaining how rmCst6 increases ERα expression is currently unknown. Previously it was proposed that ERβ may cause an upregulation of cystatins in triple negative breast cancer[47]. These cystatins may suppress canonical TGFβ signaling leading to decreased Smad2/3 phosphorylation[48]. Inactivated Smad2/3 decreases transport of Smad4, a known inhibitor of ERα transcriptional activity into the nucleus[49]. Increased ERα activity may lead to a mechanism whereby ERα regulates its own expression, leading to increased estrogen influx.

We hope that the work performed in this study will assist in the development of novel treatments focused on using recombinant CST6 to ameliorate bone resorption in MM osteolytic bone disease as well as other condition induced increased bone resorption. Here we found that increased intracellular estrogen influx in pre-osteoclastic primary BM cells treated with rmCst6 support a mechanism by which Cst6 mediates increased intracellular uptake of estrogen, leading to decreased bone resorption and increased bone formation[27-30]. Previously, loss of Cst6 was shown to negatively impact *ERα* gene expression in breast cancer. Yet, the mechanism explaining how Cst6 promotes estrogen influx is currently unknown. It is our belief that this research will lead to further studies focused on understanding the mechanism by which Cst6 is able to promote estrogen influx and suppress bone resorption. Our future efforts to understand

the mechanism by which CST6 suppresses bone resorption will be investigated through use of an ERα conditional knockout mouse model and by investigating TGFβ/Smad signaling pathways that CST6 may potentially regulate.

Material and Methods

Cell Cultures

Murine osteoclast progenitor macrophage cell line RAW 264.7 cells and bone marrow stromal cell line ST2 cells were commercially obtained (American Type Culture Collection [ATCC], Manassas, VA, http://www.atcc.org). Cells were initially cultured in Dulbeco's modified Eagle medium (DMEM) supplemented with 10% heat inactivated fetal bovine serum (FBS) and penicillin (100 µg/ml)/streptomycin (100 µg/ml) (1% P/S). MC3T3-E1 osteoblastic precursor cells were initially cultured in α-MEM, supplemented with 10% FBS, 1% P/S. ATDC5 mouse chondroprogenitor cells were purchased commercially (Sigma Aldrich, St. Louis, MO). ATDC5 cells were initially cultured in DMEM/F12 (containing 2 mM glutamine) (Corning, catalog # 10103CV) with 5% FBS and 1% P/S. For all cell types, media was changed every 2 - 3 days and cells were split when necessary to avoid over confluence.

In ex vivo, mouse bone marrow cells from flushed femur were first cultured in α-minimum essential media (αMEM) supplemented with 10% FBS, 1% P/S, and 4 mM glutamine for 24 hrs. Following this, non-adherent bone marrow cells were cultured onto tissue culture plates for analysis of intracellular estrogen concentration.

5TGM1/KaLwRij MM mouse model

Six to eight-week-old female C57BL/KaLwRij mice (Harlan Mice, Netherlands) were injected with 1×10^6 5TGM1-GFP cells intravenously via the tail vein and randomized into 3 groups (MM mice, n = 5 per group). Five days after injection of tumor cells, mice were treated with either PBS (100 µl), rmCst6 (200 µg/kg) via intravenous (i.v) injection twice a week, or Zoledronic Acid (ZA) (100 µg/kg) via subcutaneous (s.c) injection twice a week. On day 25 post-tumor cell inoculation, when most mice had started to develop paraplegia, the experiment was terminated, and mice were sacrificed. Blood samples were collected every week. All animal procedures adhered to a protocol approved by the local Institutional Animal Care and Use Committee (IACUC) at the University of Arkansas for Medical Sciences.

Recombinant CST6 (rmCst6) expression and purification

Mouse CST6-cDNAs cloned into pcDNA3.1(+)-C-6His was purchased from GenScript (Piscataway, NJ). The constructs were then transfected into HEK293T cells via Lipofectamine2000 (ThermoFisher, Cat#11668500). Conditioned media was collected 48 and 72 hrs. after transfection. The pH of the medium was adjusted to pH7.5-8.0 with 0.05 M NaOH, then loaded into the HisTrap HP column (Cytiva, Cat#17524801) using a peristaltic pump at 4 °C. The His tag proteins were washed with 50ml of 50 mM Na-Phosphate, 300 mM NaCl, 10% glycerol, 5 mM Imidazole pH 7.5, and eluted with 50 mL 0-100% to 50 mM Na-Phosphate, 300 mM NaCl, 10% glycerol, 300 mM Imidazole pH 7.5 using the NGC column Chromatography System (Bio-Rad, Hercules, CA). After concentration by ultrafiltration, 5 ml samples were loaded onto a Superdex 75 100/300 GL column (Cytiva, Cat#29148721) pre-equilibrated with 50 mM Na-Phosphate pH 7.5, 150 mM NaCl, at a flowrate of 0.75 ml/min. The protein purity was determined by silver stain according to the Pierce Silver Stain Kit protocol (ThermoFisher, Cat#24612). The concentration of the purified protein was determined at 280 nm by nanodrop 2000 (Thermo Scientific). The purified protein was tested for functionality prior to use in *in-vivo* tests.

Ovariectomy (OVX) mouse model

6-month-old female C57BL/6J mice (Jackson Laboratories) were utilized in this study. Mice were anesthetized with chloral hydrate and subjected to ovariectomy or sham operation. Following OVX surgery, mice were randomly divided into 4 groups to receive the following treatments: (1) Sham operation + PBS (Sham, n = 8), (2) OVX + PBS (OVX-PBS, n = 8), (3) 100 μg/kg Zoledronic Acid (OVX-ZA, n = 9), (4) 50 μg/kg rmCst6 (OVX-CST6, n=10). Two days following surgery, mice were administered drugs for 6 weeks via i.p, i.v, or s.c injection. OVX-ZA mice received injections twice a week while OVX-CST6 mice received injections every other day. After 6 weeks mice were sacrificed. Mouse serum, legs, and vertebras were collected and stored at -80°C until used. Successful OVX was confirmed by an assessment of uterus weight and weight development during the experiment.

Micro-computed tomography (μCT)

μCT analysis of mice tibia was performed as previously described[50]. Tibias from both MM and OVX models were dissected and fixed in 10% neutral-buffered formalin for 2 days. For μCT, region of interest (ROI) was selected to include the entire epiphysis and metaphysis of one end of the tibia as it contains trabecular bone. Scans were acquired at 60kV and 166uA; Al

0.5mm filter; 10uM Pixel size. After scanning, tibia images were reconstructed using the Skyscan NRecon program with a beam hardening correction of 40. Trabecular and cortical bone microarchitecture were analyzed using the Skyscan CT Analyzer program. The following bone parameters were calculated using μCT analysis: bone volume fraction (BV/TV%), trabecular number (Tb N, 1/mm), trabecular thickness (Tb Th, mm), trabecular separation (Tb Sp, mm), and bone mineral density (BMD).

Bone histomorphometry

Following μCT, tibia from both MM and OVX mouse models were decalcified in 5% EDTA solution (pH 7.0) for 7 days at room temperature and embedded in paraffin. Bone sections (5 μm thickness) were stained for H&E and tartrate-resistant acid phosphatase (TRAPase) staining using a Leukocyte Acid Phosphatase Kit (Sigma-Aldrich, St. Louis, MO). For the MM mouse models, histomorphometric analyses was performed using the OsteoMeasure software (OsteoMetrics,) with a Zeiss Axioskop2 microscope. For the OVX mouse models, TRAPase positive cells and adipocyte-like cells were counted using Nikon NIS elements platform and normalized to total area of ROI at 20X magnification (285474.816 μm^2). At 10X and 20X magnifications, regions were selected to include areas with minimal damage. In addition to this, regions were also chosen to include all cell and tissue types (adipocyte-like cells, TRAPase positive cells and bone matrix). For both MM and OVX mouse models, histomorphometric parameters were averaged for each treatment and graphed using GraphPad prism 9.0.

Evaluation of intracellular bone turnover markers and estrogen levels

The serum levels of CTX-1 and P1NP were examined using a CTX-1 ELISA kit and P1NP ELISA kit (Novus) according to the manufacturer's instructions for both OVX mice. Intracellular total estrogen concentration for non-adherent BMC treated with rmCst6 (100 ng/ml) or ZA (1 μM) was examined using a mouse estrogen ELISA kit (Mybiosource: MBS766177). Cells were cultured in αMEM in triplicate with treatments for 72 hrs. at 37° C. After 72 hrs., cells were lysed and assayed according to the manufacturer's instructions. Total intracellular estrogen concentration for non-adherent BMC was measured using triplicate analysis and experiment was repeated three times to give N = 9 for each treatment (Control, 1 μM ZA, 100 ng/ml rmCst6). Results for estrogen concentration (pg/ml) were normalized by dividing by intracellular protein concentration (μg/ml). To reduce variability between plates, data was normalized for each plate by dividing estrogen concentration (pg/μg) for each sample by average

estrogen concentration of control treatment for said plate, then multiplying by the average estrogen concentration for all samples across three plates. Following normalization, results were plotted using GraphPad Prism 9.0.

Single cell RNA sequencing (scRNA-seq)

scRNA-seq was performed as previously described[16]. Briefly, BM mononuclear cells from 5TGM1/KaLwRij (MM) mice were isolated were isolated at 25 days post tumor cell inoculation. Cells were isolated from healthy control mice (n = 2), MM mice (n = 3), MM mice + rmCst6 (n = 3) or MM mice + ZA (n = 2) treated mice sorted using fluorescence-activated cell sorting (FACS). Sorted GFP negative cells with a purity greater than 95% and viability higher than 95% were used for 10 X genomics scRNA-seq, resuspended in Mg- and Ca- free PBS (+0.04% BSA) and counted using a light microscope under 10X magnification. Single-cell emulsions were generated (Chromium Controller, Chromium Next GEM Chip G, Chromium NextGEM Single Cell 3' v3.1 kit; 10X Genomics, Pleasanton, CA, USA). Libraries were assessed for mass concentration, fragment size and validated. Initial sequencing was performed on an Illumina NovaSeq SP 100-cycle flow cell and data was assessed using the Cell Ranger Count output.

Bioinformatic analysis of scRNA-seq

Bioinformatics analysis of scRNA-seq data was performed as previously described[16]. Briefly, raw sequencing fastq files were processed using CellRanger software (10X Genomics) version 6 with *Mus musculus* reference genome. The count table was loaded into R through Seurat version 4 package for further analysis. Cells with gene numbers less than 500, greater than 5000 and more than 10% of unique molecular identifiers from mitochondrial genes were discarded from the analysis. Principal component (PCA) was performed on significantly variable genes from remaining cells. Nitration results were used as input for clustering using Louvain algorithm with multilevel refinement and Uniform Manifold Approximation and Projection for Dimension Reduction (UMAP). Gene specific markers of each cluster were identified using the FindMarkersAll function with MAST method test statistics. Cell clusters and gene markers include mature neutrophils-I (*S100a8, Ly6g*), mature neutrophils-II (*Rethlg, MMP9*), immature neutrophils-I (*Chil3, Camp*), macrophages (*Adgre1, Mafb*), monocyte prog-I (*F13a1, Itga1*), monocyte prog-II (*Prtn3*, *Hsp90ab1*), dendritic cells (*Siglech, Bst2, Tcf4*), lymphomyeloids prog-I (*Irf8, Flt3*), myeloid prog (*Mpo*, *Cd63*), immature neutrophils-II (*Cenbf, Camp*), B cells

(*Ighm, Cd79b*), NK/T cells (*Cd3e, Gzmb*), immature neutrophils-III (*Fcnb, Camp*), monocytes (*ly6c2, ccl2*), pre/pro B cells (*Pax-5, Vpreb3*), lymphomyeloids prog-II (*Atp2b4, Hlf*) and eosinophil/basophil prog (*Gata2, Cpa3*).

To visualize genes simultaneously in kernel joint density estimation, the Nebulosa package was used. Based on the kernel joint density of Adgr1 and Fcgr3, we sub-selected cells that have a high value of the kernel joint density for subclustering analysis to study the cellular heterogeneity of macrophage cells. Gene-set enrichment analysis of marker genes was performed on Gene Ontology annotation using piano package.

***In ex vivo* osteoclast differentiation**

Primary mouse BM cells were flushed out from the femur and tibia 6-8-week C57BL/6J mice, BM erythrocytes were removed with the ACK Lysing Buffer (KD Medical, catalog # RGF3015) for 3 min. The remaining cells were cultured in α-MEM (Gibco, catalog # 12571048) supplemented with 10% FBS and 10 ng/ml M-CSF (PeproTech, catalog # 315-02) overnight in 10 cm tissue culture dish. 4 x 10^4 non-adherent cells were seeded into 96-well plate with α-MEM containing 10% FBS and 10 ng/ml M-CSF for 3 days to recruit macrophage and then osteoclast differentiation was induced by addition of 10 ng/ml RANKL (R&D, catalog # 462-TEC-010/CF) with or without rmCst6 protein or ZA for 3-5 days. Media changes were carried out every 2 days. After 3 days the cells were evaluated for TRAP staining.

Osteoblast and chondrocyte precursor histological staining

Osteoblast precursors MC3T3-E1 were seeded at 15,000 cells/cm^2 in 12-well or 24-well plates (α-MEM, supplemented with 10% FBS, 1% P/S). At 80% confluence, the media was changed to osteogenic induction media (α-MEM, supplemented with 10% FBS, 1% P/S, 50 μg/ml L-Ascorbic Acid (Sigma-Aldrich, catalog # A5960) and 5 mM β-Glycerophosphate (Sigma-Aldrich, catalog # 9422). Media was changed every 2–3 days during the culture period. On day 14, the activity of alkaline phosphatase (ALP) was evaluated using histological staining. Cells were washed with PBS and fixed with 4% paraformaldehyde for 20 min at room temperature, and then stained with 1-step NBT-BCIP substrate solution (Thermo Scientific, catalog # 34042) for 20 minutes. After staining, cells were washed twice with water and observed under a light microscope. On day 21, cells were fixed and stained with 2% Alizarin Red (Sigma-Aldrich, catalog # A5533) at pH 4.2 to evaluate the mineralization using previously described methods[51].

ATDC5 mouse chondroprogenitor cells were purchased commercially (Sigma Aldrich, St. Louis, MO). ATDC5 cells were initially cultured in DMEM/F12 (containing 2 mM glutamine) (Corning) with 5% FBS and 1% penicillin/streptomycin (P/S). For chondrocyte mineralization, cells were initially seeded at 15,000 cells/cm^2. At 80% confluence, the media was changed to chondrocyte differentiation media comprised of DMEM/F12 (containing 2 mM glutamine) (Corning) with 5% FBS, 1% P/S and 1 X insulin-transferrin-selenium (ITS) (ThermoFisher, catalog # 41400045) and cells were treated with either 200 ng/ml rmCst6 or ZA (0.5 µM, 1 µM, 2 µM). The media was changed every 2-3 days during the culture. After 14 days cells were washed with PBS, fixed with 4% paraformaldehyde (20 min, room temperature) and then stained with Alcian blue staining solution (Sigma Aldrich, catalog # TMS-010-C) for 30 min at room temperature[51]. After staining, cells were washed twice with water and observed under a light microscope. On day 21, ATDC5 cells were fixed and stained with 2% Alizarin Red (Sigma-Aldrich, catalog # A5533) at pH 4.2 to evaluate the mineralization[51].

Cell counting kit (CCK)-8 assay

2,000 cells (either ATDC5 or MC3T3-E1 cell line) seeded in 96 well plate in 100 µl culture medium were allowed to adhere overnight and then were treated with different doses of Zoledronic Acid (0-20 µM) for 7 days in a humidified atmosphere of 5% CO2 at 37˚C. Following treatment, 10 µl CCK-8 solution (Apexbio Technology, catalog # K10181) was added to each well and the plate was incubated for 2 hours in the incubator. The absorbance was measured at a wavelength of 450 nm using a microplate reader (BioTek, USA). Results were averaged and plotted using GraphPad Prism 9.0.

Cytokine array

RayBio C-Series Mouse Cytokine antibody array C1000 (RayBiotech) was used according to the manufacturer's protocol with protein lysate from ovariectomized mice L3-L5 vertebrae. Protein was isolated from vertebrae by homogenization with RIPA buffer (Solarbio) followed by sonication. Protein concentrations were found for lysates using BCA assay and for each treatment samples were pooled. Final concentration for each pooled sample was 1.94 mg/ml. Samples were added to array membrane in triplicate according to the manufacturer's protocol. A heat map (GraphPad Prism 9.0) was created for array targets where CST6 or ZA treatments were shown to reduce cytokine levels elevated by OVX to near sham levels.

RNA isolation, real-time reverse transcription-polymerase chain reaction

For measurement of *Slco1a4* mRNA levels, Raw 264.7 cells (20 ng/ml RANKL) or ST2 cells were cultured into 12 well tissue culture plates (2.5 x 10^5 cells/ml, 1 ml total volume). Cells were treated with either a PBS control solution or increasing concentrations of rmCst6 (50 ng/ml, 100 ng/ml or 200 ng/ml). Cells were incubated at 37° C for 72 hr. For ST2 cells incubated with ascorbate-2-phosphate (A2P), cells were initially cultured at 2000 cells/well and incubated at 37°C for 10 days, with the same treatments applied. Media and treatments were replaced every 48 hr. For measurement of *ERα* mRNA levels Raw 264.7 cells were cultured into 12 well tissue culture plates (2.5 x 10^5 cells/ml, 1 ml total volume), treated with PBS control solution, 1 μM ZA, or 100 ng/ml rmCst6 (+/- 20 ng/ml RANKL) and incubated at 37° C for 48 hr.

For each treatment, triplicate samples were cultured. RNA was isolated using RNeasy plus Mini Kit from Qiagen. RNA concentration and purity (A260/A280) for RNA samples were determined using a Polarstar Omega plate reader. Reverse transcription was carried out using an iScript cDNA Synthesis Kit. Real-time polymerase chain reaction (RT-PCR) experiment was carried out using SYBR Green and with the QuantStudio 6 Flex real-time PCR system from Applied Biosystems. Samples were performed in triplicate, and gene expression was normalized to cyclophillin A and averaged for each treatment concentration. ERα, Slco1a4 and cyclophillin A primers for RT-PCR analysis were designed using Primer Express Software 2.0.0.

For analysis of basal *Slco1a4* tissue and cell mRNA levels RNA was isolated from the following tissues using the trizol method: tibia, L3-L5 vertebrae, bone marrow cells, and empty femur as well as from the following cell types Raw 264.7, ST2, OB6, ATDC5 and MLOY4 and purified using RNeasy plus Mini Kit. RNA concentration and purity (A260/A280) for RNA was determined as previously described and cDNA was synthesized. QuantStudio 6 Flex real-time PCR system was used for determining basal expression in tissues and cell culture. Following real-time PCR, gene expression was then visualized using agarose gel electrophoresis.

For *in vivo* analysis of Slco1a4 and ERα mRNA levels total RNA was isolated from mouse L3-L5 vertebrae for all samples from each treatment group (Sham, OVX-PBS, OVX-CST6, OVX-ZA). Tissue was first homogenized using metal beads and a homogenizer (6500 rpm, 20 seconds, twice). After homogenization, total RNA was isolated using trizol and purified using the RNeasy plus Mini Kit. For real time PCR, RNA concentration and purity was determined as with previous RNA samples and cDNA was synthesized using using iScript cDNA Synthesis Kit. RT-PCR experiment was carried out using SYBR Green as described in the

above paragraphs with gene expression being normalized to cyclophillin A. For all RT-PCR experiments, results were averaged and graphed using GraphPad Prism 9.0.

Bone tissue RNA sequencing analysis

For RNA sequencing experiments, RNA was isolated from *in vivo* (tibia; OVX mouse model; Sham, OVX-PBS, OVX-CST6, OVX-ZA; three samples per group) samples as described earlier. R12NA integrity was checked using Agilent Technologies 4200 Tapestation with RNA screen tape. Samples with RIN^e greater than 8 were used for further analysis. RNA sequencing was performed in the UAMS developmental genomics core. Briefly, Sequence ready libraries were constructed using the Illumina Stranded mRNA Prep Ligation kit following the manufacturer's protocol, then sequenced on an Illumina NextSeq 500. Briefly, poly-A containing mRNA was isolated from total RNA using oligo-dt attached magnetic beads and then converted to cDNA. After fragmentation and end repair, cDNA 3' ends were adenylated and then ligated with index anchors. The anchor ligated fragments were indexed and amplified, then normalized, pooled and sequenced.

Analysis of RNA sequencing results was performed at the Louisiana Cancer Research Center. Briefly, FASTQ files were uploaded to Partek Flow and contaminants were removed with Bowtie 2 (v2.2.5). Reads were aligned to STAR v2.7.8a using the mm10 version of the mouse genome. Aligned reads were quantified using Ensembl Transcripts release 102. Features with a maximum reads ≤ 5 were filtered out from the analysis. Normalization was done by TMM and log2 transformation. Pathway analysis (KEGG) was performed in Partek Flow. Heat maps comparing LS mean for treated samples (OVX-CST6, OVX-ZA) to OVX samples were created using GraphPad Prism 9.0.

Western blots

To analyze ERα protein expression, total protein from each sample was first isolated from L3-L5 vertebrae by homogenization with RIPA buffer (Solarbio) followed by sonication. Protein concentrations were found for lysates using BCA assay. For ERα protein expression in Raw 264.7 cells (+/- 20 ng/ml RANKL) cells were cultured onto 6 well tissue culture plates with either control, 1 μM ZA or 100 ng/ml rmCst6 treatments and incubated at 37° C for 48 hr. (2.5 x 10^5 cells/ml, 2 ml total volume). After 48 hr. cells were lysed using RIPA buffer and protein concentration was found using BCA assay. Both protein tissue and protein cell samples were prepared for SDS PAGE, equal amount of protein were loaded for each sample and then ran on

10% Acrylamide/Bis-acrylamide gels (N = 6 for bone tissue, N = 3 for Raw 264.7 cells). Following membrane transfer, mouse anti h/m/r ERα (MAB57151, R&D Systems) was used as the primary antibody and HRP conjugated anti-mouse IgG (R&D systems, HAF018) was used as the secondary antibody. Bands of interest were visualized and imaged under chemiluminescent detection using the Amersham Imager 600 System. Amido black staining (for tissue lysate samples) and mouse anti β-actin antibody (Sigma, A1978) (for cell lysate samples) were used as loading controls for western blots. Densitometry analysis of western blot bands was performed using ImageJ.

Immunohistochemistry

Raw 264.7 cells were grown to 10,000 cells/well in Nunc. Lab Tec Chamber slides (Thermo Fisher, 177399) in DMEM supplemented with 10% FBS and 1% P/S. Cells were treated with either control solution or 100 ng/ml rmCst6 and incubated at 37° C for either 24 hr. or 7 days. 7-day incubation period was in the presence of 20 ng/ml RANKL. Following incubation, immunostaining was performed as follows. Media was aspirated and cells were rinsed with cold 4% paraformaldehyde in 1X PBS and incubated at room temperature for 1 min. Cells were then fixed with 4% paraformaldehyde in 1X PBS at room temperature for 20 min. Paraformaldehyde was removed and cells were rinsed with 1X PBS. Cells were then covered with 1X PBS (10 – 15 min., room temperature). PBS was removed and 2.5% Horse Blocking serum was added (20 min., room temperature). After 20 min. blocking serum was removed via aspiration and cells were incubated with primary antibody (ERα : Millipore, MAB447; PPARγ: abcam, ab191407) diluted 1:50 in 2.5% horse blocking serum containing 1% IGEPAL) overnight at 4° C. Cells were then washed with 1X PBS containing 0.05% IGEPAL (3 min., 3 times at room temperature) and secondary antibody was added (ERα : abcam, ab150105, PPARγ: abcam, ab150067) (1 hr., room temperature, protected from light). Cells were washed with 1X PBS containing 0.05% IGEPAL again (3 min., 3 times at room temperature, protected from light). Final cells were covered with DAPI-Fluoromount-G and observed using Nikon Eclipse T/2 epifluorescent microscope.

Statistical analysis

Statistical analysis was performed with GraphPad Prism 9.0 (GraphPad Software, Inc., San Diego, Ca, USA). Numerical variables were expressed as mean ± SD (Standard Deviation); n equals to the number of samples/group. For all experiments differences within groups were

evaluated using either one-way ANOVA or t-test followed by Turkey's post hoc test. Values were considered statistically significant at $p < .05$.

Study approval

The animal studies were performed according to the guidelines of the Institutional Animal Care and local veterinary office and ethics committee of the UAMS under approved protocol (IACUC 3991 and 4090). De-identified primary samples were obtained from myeloma patients during UAMS clinic visits. Signed institutional review board-approved informed consent forms are kept on record in UAMS Tissue Biorepository and Procurement Service (TBAPS) under approved protocol IRB # 262254 and 260887. Peripheral blood from healthy donors were collected using UARK protocol 2009-88 under IRB# 5455.

Conflict of Interest:

The authors have declared that no conflict of interest exists.

Author contributions

Study conceived and planned by J.R.C. and F.Z.; D.G., P.C.C., and J.R.C. wrote the paper. J.R.C. and F.D. are senior authors designed and performed the study; cell, biochemical and molecular *in ex vivo* and *in vitro* experimental works by D.G., P.C.C., O.P.L., M.L.B., J.F.C., C.E.R., Z.Z., Y.C., F.S., H.W., data analysis by J.R.C., J.F.C., D.G., P.C.C., F.Z.; manuscript composition by J.R.C., J.F.C. P.C.C.; all authors discussed the results and edited the manuscript.

Acknowledgement:

Supported by National Cancer Institute 1R01CA236814-01A1, 3R01-CA236814-03S1, and U54CA272691-01, U.S. Department of Defense (CA180190), the Myeloma Solution Fund (MSF), as well as funding from the Myeloma Crowd Research Initiative Award and the Paula and Rodger Riney Foundation, and UAMS Winthrop P. Rockefeller Cancer Institute (WRCRI) Fund to FZ. And, in part by National Institute of Health grant R37 AA18282 sub-award to JRC.

Competing interests

The authors declare no competing interests.

References Cited

1. Kumar, S. K. et al. Multiple myeloma. *Nature Reviews Disease Primers*. **3**, 1–20 (2017).

2. Roodman, G. D. Pathogenesis of myeloma bone disease. *Leukemia.* **23**, 435–441 (2009).

3. Tian, E. et al. The role of the wnt-signaling antagonist DKK1 in the development of osteolytic lesions in multiple myeloma. *N Engl J*. **349**, 2483–2494 (2003).

4. Terpos, E., Ntanasis-Stathopoulos, I. & Dimopoulos, M. A. Myeloma bone disease: from biology findings to treatment approaches. *Blood*. **133**, 1534–1539 (2019).

5. Pozzi, S. et al. High-dose zoledronic acid impacts bone remodeling with effects on osteoblastic lineage and bone mechanical properties. *Clinical Cancer Research*. **15**, 5829–5839 (2009).

6. Bone, H. G. et al. Ten Years' Experience with alendronate for osteoporosis in postmenopausal women. *N Engl J*. **350**, 1189–1199 (2004).

7. Aapro, M. et al. Guidance on the use of bisphosphonates in solid tumours: recommendations of an international expert panel. *Annals of Oncology*. **19**, 420–432 (2008).

8. Van Beek, E., Pieterman, E., Cohen, L., Löwik, C. & Papapoulos, S. Farnesyl pyrophosphate synthase is the molecular target of nitrogen-containing bisphosphonates. *Biochem Biophys Res Commun*. **264**, 108–111 (1999).

9. Dunford, J. E., Rogers, M. J., Ebetino, F. H., Phipps, R. J. & Coxon, F. P. Inhibition of protein prenylation by bisphosphonates causes sustained activation of Rac, CDC42, and Rho GTPases. *JBMR.* **21**, 684–694 (2006).

10. Huang, X. et al. Dose-dependent inhibitory effects of zoledronic acid on osteoblast viability and function in vitro. *Mol Med Rep*. **13**, 613 (2016).

11. Raje, N. et al. Clinical, radiographic, and biochemical characterization of multiple myeloma patients with osteonecrosis of the jaw. *Clinical Cancer Research.* **14**, 2387–2395 (2008).

12. Terpos, E., Roodman, G. D. & Dimopoulos, M. A. Optimal use of bisphosphonates in patients with multiple myeloma. *Blood*. **121**, 3325–3328 (2013).

13. Terpos, E., Ntanasis-Stathopoulos, I., Gavriatopoulou, M. & Dimopoulos M. A. Pathogenesis of bone disease in multiple myeloma: from bench to bedside. *Blood Cancer J*. **8**, 7 (2018).

14. Paton-Hough, J. et al. Preventing and repairing myeloma bone disease by combining conventional antiresorptive treatment with a bone anabolic agent in murine models. *JBMR*. **34**, 783 (2019).

15. Nyman, J. S. et al. Combined treatment with a transforming growth factor beta inhibitor (1D11) and bortezomib improves bone architecture in a mouse model of myeloma-induced bone disease. *Bone.* **91**, 81–91 (2016).

16. Gai, D. et al. CST6 suppresses osteolytic bone disease in multiple myeloma by blocking osteoclast differentiation. *J Clin Invest.* **132**, 159527 (2022).

17. Li, X. et al. CST6 protein and peptides inhibit breast cancer bone metastasis by suppressing CTSB activity and osteoclastogenesis. *Theranostics*. **11**, 9821 (2021).

18. Ko, E. et al. Cystatin M loss is associated with the losses of estrogen receptor, progesterone receptor, and HER4 in invasive breast cancer. *Breast Cancer Res*. **12**, R100 (2010).

19. Tsukasaki, M. et al. Stepwise cell fate decision pathways during osteoclastogenesis at single-cell resolution. *Nature Metabolism.* **2**, 1382–1390 (2020).

20. Kalish, S. et al. M3 macrophages stop division of tumor cells in vitro and extend survival of mice with ehrlich ascites carcinoma. *Med Sci Monit Basic Res*. **23**, 8 (2017).

21. Newton, P. T. et al. Chondrogenic ATDC5 cells: An optimized model for rapid and physiological matrix mineralization. *Int J Mol Med*. **30**, 1187 (2012).

22. Tai, T. W. et al. Reactive oxygen species are required for zoledronic acid-induced apoptosis in osteoclast precursors and mature osteoclast-like cells. *Sci Rep.* **7**, 1–12 (2017).

23. Chen, Y. et al. Apoptotic effect of matrix metalloproteinases 9 in the development of diabetic retinopathy. *Int J Clin Exp Pathol*. **8**, 10452 (2015).

24. Lee, W. et al. Polymorphisms in human organic anion-transporting polypeptide 1A2 (OATP1A2): Implications for altered drug disposition and central nervous system drug entry. *JBC*. **280**, 9610–9617 (2005).

25. Leuthold, S. et al. Mechanisms of pH-gradient driven transport mediated by organic anion polypeptide transporters. *Am J Physiol Cell Physiol*. **296**, 570–582 (2009).

26. Cho, E., Montgomery, R. B. & Mostaghel, E. A. Minireview: SLCO and ABC transporters: A role for steroid transport in prostate cancer progression. *Endocrinology.* **155**, 4124 (2014).

27. Norton, A., Thieu, K., Baumann, C. W., Lowe, D. A. & Mansky, K. C. Estrogen regulation of myokines that enhance osteoclast differentiation and activity. *Sci Rep*. **12**, 15900 (2022).

28. Streicher, C. et al. Estrogen regulates bone turnover by targeting RANKL expression in bone lining cells. *Sci Rep*. **7**, 1-14 (2017).

29. Gavali, S. et al. Estrogen enhances human osteoblast survival and function via promotion of autophagy. *BBA - Molecular Cell Research*. **1866**, 1498–1507 (2019).

30. Matsumoto, Y. et al. Estrogen and glucocorticoid regulate osteoblast differentiation through the interaction of bone morphogenetic protein-2 and tumor necrosis factor-α in C2C12 cells. *Mol Cell Endocrinol*. **325**, 118–127 (2010).

31. Mohamad, N. V., Ima-Nirwana, S. & Chin, K. Y. Are oxidative stress and inflammation mediators of bone loss due to estrogen deficiency? A review of current evidence. *Endocr Metab Immune Disord Drug Targets*. **20**, 1478-1487 (2020).

32. Baek, K. H. et al. Association of oxidative stress with postmenopausal osteoporosis and the effects of hydrogen peroxide on osteoclast formation in human bone marrow cell cultures. *Calcif Tissue Int*. **87**, 226–235 (2010).

33. Giannoni, E. et al. Estradiol and progesterone strongly inhibit the innate immune response of mononuclear cells in newborns. *Infect Immun*. **79**, 2690–2698 (2011).

34. Dou, C. E. et al. Estrogen deficiency-mediated M2 macrophage osteoclastogenesis contributes to M1/M2 ratio alteration in ovariectomized osteoporotic mice. *JBMR*. **33**, 899-908 (2017).

35. Magister, Š. & Kos, J. Cystatins in immune system. *J Cancer*. **4**, 45-46. (2013)

36. Redza-Dutordoir, M. & Averill-Bates, D. A. Activation of apoptosis signaling pathways by reactive oxygen species. *BBA - Molecular Cell Research*. **1863**, 2977–2992 (2016).

37. Yang, K. et al. YAP and ERK mediated mechanical strain-induced cell cycle progression through RhoA and cytoskeletal dynamics in rat growth plate chondrocytes. *Journal of Orthopaedic Research*. **34**, 1121–1129 (2016).

38. Singhatanadgit, W., Hankamolsiri, W. & Janvikul, W. Geranylgeraniol prevents zoledronic acid-mediated reduction of viable mesenchymal stem cells via induction of Rho-dependent YAP activation. *R Soc Open Sci*. **8**, 202066 (2021).

39. Lei, Z., Xiaoying, Z. & Xingguo, L. Ovariectomy-associated changes in bone mineral density and bone marrow haematopoiesis in rats. *Int J Exp Pathol*. **90**, 512-519 (2009).

40. Homma, H. et al. Estrogen suppresses transcription of lipoprotein lipase gene: Existence of a unique estrogen response element on the lipoprotein lipase promoter. *JBC*. **275**, 11404–11411 (2000).

41. An, J. et al. Estradiol repression of tumor necrosis factor-α transcription requires estrogen receptor activation function-2 and is enhanced by coactivators. *PNAS*. **96**, 15161–15166 (1999).

42. Dragin, N. et al. Balance between estrogens and proinflammatory cytokines regulates chemokine production involved in thymic germinal center formation. *Sci Rep*. **7**, 7970 (2017)

800 43. Figueira, M. I. et al. Estrogens down-regulate the stem cell factor (SCF)/c-KIT system in
801 prostate cells: Evidence of antiproliferative and proapoptotic effects. *Biochem Pharmacol*.
802 **99**, 73–87 (2016).

803 44. Arun, M. Z. et al. Zoledronate upregulates MMP-9 and -13 in rat vascular smooth muscle
804 cells by inducing oxidative stress. *Drug Des Devel Ther*. **10**, 1453 (2016).

805 45. Kuroshima, S., Go, V. A. A. & Yamashita, J. Increased numbers of nonattached
806 osteoclasts after long-term zoledronic acid therapy in mice. *Endocrinology*. **153**, 17
807 (2012).

808 46. Richardson, H. et al. Baseline estrogen levels in postmenopausal women participating in
809 the MAP.3 breast cancer chemoprevention trial. *Menopause*. **27**, 693–700 (2020).

810 47. Sellitto, A. et al. Insights into the Role of Estrogen Receptor β in Triple-Negative Breast
811 Cancer. *Cancers (Basel)*. **12**, 1477 (2020)

812 48. Band, A. M. & Laiho, M. Crosstalk of TGF-β and estrogen receptor signaling in breast
813 cancer. *J Mammary Gland Biol Neoplasia*. **16**, 109–115 (2011).

814 49. Wu, L. et al. Smad4 as a transcription corepressor for estrogen receptor α. *JBC*. **278**,
815 15192–15200 (2003).

816 50. Caviness, P. C. et al. Phenolic acids prevent sex-steroid deficiency-induced bone loss and
817 bone marrow adipogenesis in mice. *J Nutr Biochem*. **127**, 109601 (2024).

818 51. Chen, J. R., Zhao, H., Lazarenko, O. P., Blackburn, M. L. & Shankar, K. Maternal
819 regulation of SATB2 in osteo-progeniters impairs skeletal development in offspring.
820 *FASEB J*. **34**, 2511-2323 (2019).

821

822 **Table 1:** Lesion number and μCT parameters calculated for MM mouse models (n=5)

	MM	**MM+rmCST6**	**MM+ZA**
Lesion Number	19.2 +/- 4.2	12.6 +/- 2.8	4.4 +/- 0.9
BV/TV (%)	2.64 +/- 0.52	3.57 +/- 0.14	3.88 +/- 0.53
Tb. N (1/mm)	0.56 +/- 0.09	0.82 +/- 0.02	0.85 +/- 0.12
Tb. Th (mm)	0.047 +/- 0.004	0.044 +/- 0.002	0.045 +/- 0.0008

Tb. Sp (mm)	0.45 +/- 0.06	0.38 +/- 0.02	0.38 +/- 0.025
BMD (g/cm^3)	0.072 +/- 0.01	0.10 +/- 0.008	0.12 +/- 0.012

823

824 **Table 2:** μCT parameters calculated for OVX mouse models (n=7)

	Sham	**OVX**	**OVX + rmCST6**	**OVX + ZA**
BV/TV (%)	3.1 +/- 0.6	2.2 +/- 0.40	3.3 +/- 0.43	3.84 +/- 0.23
Tb. N (1/mm)	0.64 +/- 0.08	0.50 +/- 0.10	0.70 +/- 0.078	0.86 +/- 0.053
Tb. Th (mm)	0.049 +/- 0.002	0.043 +/- 0.002	0.043 +/- 0.0008	0.04 +/- 0.001
Tb. Sp (mm)	0.37 +/- 0.03	0.39 +/- 0.01	0.31 +/- 0.01	0.37 +/- 0.014
BMD (g/cm^3)	0.087 +/- 0.015	0.052 +/- 0.0068	0.079 +/- 0.008	0.10 +/- 0.007

825

826 **Table 3:** Cytokine array data and statistical analysis (n=3).

Protein	Sham Average	OVX-PBS Average	OVX-CST6 Average	OVX-ZA Average	T-test Sham vs OVX-PBS	T-test OVX-CST6 vs OVX-PBS	T-test OVX-ZA vs OVX-PBS
BLC (CXCL13)	0.41 +/- 0.14	1.39 +/- 0.25	0.54 +/- 0.14	0.46 +/- 0.03	0.004	0.004	0.001
MIP-1 alpha (CCL3)	0.55 +/- 0.27	1.39 +/- 0.78	0.64 +/- 0.05	0.70 +/- 0.09	0.07	0.08	0.10
MIP-3 alpha (CCL20)	0.51 +/- 0.12	1.22 +/- 0.27	0.73 +/- 0.08	0.71 +/- 0.05	0.01	0.13	0.13
SCF	0.72 +/- 0.17	1.42 +/- 0.04	0.69 +/- 0.13	0.74 +/- 0.096	0.001	0.000	0.000
TARC (CCL17)	0.50 +/- 0.16	1.02 +/- 0.27	0.59 +/- 0.10	0.68 +/- 0.19	0.03	0.03	0.07
TECK (CCL25)	0.61 +/- 0.37	1.17 +/- 0.26	0.50 +/- 0.05	0.57 +/- 0.17	0.05	0.007	0.01
TIMP-1	0.68 +/- 0.14	1.01 +/- 0.06	0.38 +/- 0.03	0.46 +/- 0.12	0.02	0.000	0.001
TNF alpha	0.53 +/- 0.10	1.44 +/- 0.50	0.65 +/- 0.05	0.79 +/- 0.04	0.01	0.027	0.04
TPO	0.60 +/- 0.27	1.27 +/- 0.27	0.63 +/- 0.02	0.68 +/- 0.06	0.02	0.008	0.01

827

828 **Table 4**: Western blot data and statistical analysis for Raw 264.7 cells (48 hr. incubation,
829 Control, 1 μM ZA or 100 ng/ml rmCst6 treatment) (n=3).

	Control Average	ZA Average	100 ng/ml CST6 Average	t-test Control vs ZA	t-test Control vs 100 ng/ml CST6	t-test ZA vs 100 ng/ml CST6
ERα band Intensity	13735.0 +/- 3336.7	15366.5 +/- 7562.1	24189.5 +/- 5269.1	0.37	0.021	0.086
β-actin band Intensity	11835.3 +/- 877.9	13207.1 +/- 837.6	13846.5 +/- 2350.0	0.06	0.11	0.34
ERα/β-actin	1.18 +/- 0.32	1.17 +/- 0.63	1.89 +/- 0.39	0.48	0.036	0.084

830

831 **Table 5**: Western blot data and statistical analysis for Raw 264.7 cells (48 hr. incubation, 20
832 ng/ml RANKL) Control, 1 μM ZA or 100 ng/ml rmCst6 treatment) (n=3).

	Control Average	ZA Average	100 ng/ml CST6 Average	t-test Control vs ZA	t-test Control vs 100 ng/ml CST6	t-test ZA vs 100 ng/ml CST6
ERα band Intensity	20647.3 +/- 2366.8	24660.8 +/- 1917.5	29535.7 +/- 3279.3	0.042	0.0094	0.045
β-actin band Intensity	16643.0 +/- 1369.6	17405.5 +/- 588.6	17153.1 +/- 1755.3	0.21	0.35	0.41
ERα/β-actin	1.23 +/- 0.077	1.41 +/- 0.096	1.74 +/- 0.37	0.033	0.041	0.10

833

Figure Legend

Figure 1: rmCst6 protein and ZA inhibit bone destruction in 5TGM1-C57BL/KaLwRij MM mice. (**A**) A schematic model for the MM mouse study. 5TGM1 murine MM cells were injected into 8-week-old C57BL/KaLwRij female mice via tail vein. Recombinant mouse Cst6 (rmCst6) protein and ZA were administered on day 5 post tumor inoculation. At day 25, mice were sacrificed and samples were collected. (**B**) Reconstructed μCT images of tibia sagittal sections taken from MM mice show trabecular architecture change in bone for MM mice and MM mice treated with either rmCst6 or ZA. (**C**) Bar-plots present the number of bone lytic lesions on the right medial tibia surface and the trabecular bone parameters: BV/TV, Tb.N, Tb.Th, Tb.Sp, and BMD (N=5). (**D**) Best representative images of TRAPase staining shows TRAP positive cells (indicated with arrows) in tibiae derived from C57BL/KaLwRij mice injected with 5TGM1 MM cells with or without rmCst6 and ZA treatment. (**E**) Bar-plots represent histomorphometric analyses of TRAPase-stained number of osteoclast per bone perimeter (N.Oc/B.Pm) and osteoclast surface per bone surface (Oc.S/BS) (N=5). (**F**) Representative flow cytometry plots presented the GFP + 5TGM1 cells in BM of control and rmCst6 and ZA treated mice. (**G**) Bar-plots represent the percentage of GFP+ 5TGM1 cells in BM (N=5). (**H**) Tumor burden was assessed by measuring serum levels of IgG2b (mg/ml) by ELISA (N=5). (**I**) Bar-plots show serum levels of the bone resorption marker CTX-1 detected by ELISA (N=5). For all measurements data is represented as mean ± SD and was analyzed by one-way ANOVA with Tukey's multiple-comparisons. Denoted markings are considered significant $*P < 0.05$, $**P < 0.01$, $***P < 0.001$.

Figure 2: rmCst6 protein and ZA suppress bone resorption in sex steroid deficient ovariectomized (OVX) mouse model. (**A**) A schematic model for the OVX mice study. Six-month female mice OVX were administered rmCst6 protein or ZA for 6 weeks by i.v or s.c injection twice a week. After 6 weeks, mice were sacrificed and samples were collected. (**B**) Reconstructed μCT images of tibia from OVX mice show trabecular architecture change in bone following sex steroid depletion and treatment with either rmCst6 or ZA. (**C**) Bar-plots show the trabecular bone parameters: BV/TV, Tb N, Tb Th, Tb Sp, and BMD (N=7). (**D**) Best representative images of TRAPase staining shows TRAPase positive cells (indicated with arrows) and adipocyte-like cells present in tibia from Sham, OVX, OVX + ZA and OVX + rmCst6 mice. (**E**) Bar-plots represents the histomorphometric analyses of the number of

TRAPase positive cells in the tibia normalized to total area of ROI at 20X. Number of TRAPase positive cells/μm^2 is increased only with ZA treatment (N=8). (**F**) Average number of adipocyte-like cells/μm^2 show that adiposity in bone marrow is increased following OVX, but brought back to near sham levels by rmCst6 or ZA treatment (N=8). (**G-H**) Bar-plots show the serum levels of the bone resorption marker CTX-1 and bone formation marker P1NP detected by ELISA from each group are recovered to near or better than sham levels following rmCst6 or ZA treatment (N=9). Data shown as mean +/- SD. Statistical analysis was performed using one-way ANOVA. Denoted markings are considered significant *p<0.05, **p<0.01, ***p<0.001, ****p<0.0001.

Figure 3: scRNA-seq reveals BM microenvironment alterations after rmCst6 and ZA treatment. (**A**) Experimental workflow for scRNA-seq on BM mononuclear cells. 5TGM1-GFP+ MM cells were injected into 8-week-old C57BL/KaLwRij female mice via tail intravenously. Hind limbs were extracted, and BM mononuclear cells from individual mice were sorted out by depleting 5TGM1-GFP+ MM cells. (**B**) The Uniform Manifold Approximation and Projection (UMAP) plot of BM mononuclear cells derived from control mice (n = 2), MM mice treated with PBS (n = 3), rmCst6 protein (n = 3) or ZA (n = 2). (**C**) Bar-views show the proportion of various cell types in BM mononuclear cells of control or MM-bearing mice treated with PBS, rmCst6 or ZA protein.

Figure 4: The effects of CST6 and ZA on the viability and differentiation of osteoclast, osteoblast and chondrocyte. (**A**) Mouse osteoclast precursors were differentiated into osteoclasts by addition of M-CSF and RANKL. Different concentrations of rmCst6 protein and ZA were added into the culture media for 4 days. TRAPase staining shows osteoclasts containing multiple nuclei. (**B**) Bar-plots show the quantification of $TRAP^+$ osteoclasts (n=4). (**C**) MC3T3-E1 cells were differentiated to osteoblasts with 50 μg/ml ascorbic acid and β-glycerophosphate. Alkaline phosphatase staining on day 14 (upper panel) and Alizarin red staining on day 21 (lower panel) showed ZA but not CST6 inhibited osteoblast differentiation and mineralization. (**D**) MC3T3-E1 cells were incubated with different doses of ZA for 7 days and cell viability was detected by CCK-8 assay (n=4). (**E**) ATDC5 cells were differentiated to chondrocytes with ITS medium for 14 days, Alcian blue staining (upper panel) showed the glycosaminoglycan (GAG) deposition was suppressed by ZA; ATDC5 cells were induced with 1X ITS medium plus ZA or CST6 for 21days. Endochondral ossification was detected by Alizarin red staining (lower panel). (**F**) ATDC5 cells were incubated with different doses of ZA for 7 days and cell viability was

detected by CCK-8 assay (n=4). Data shown as mean +/- SD. Statistical analysis was performed using one-way ANOVA. Denoted markings are considered significant *p<0.05, **p<0.01, ***p<0.001, ****p<0.0001.

Figure 5: OVX-induced increase in inflammatory cytokine expression is brought back to sham levels by treatment with either rmCst6 or ZA. Inflammatory cytokine array for Protein samples from L3-L5 mice vertebrae. The 25 targets with the largest initial change in membrane intensity from the sham surgery group to the OVX-PBS group are shown. Ovariectomy causes the upregulation of multiple inflammatory cytokines, which in turn can cause increased bone resorption. Treatment with either rmCst6 or ZA brought levels back to sham. For each group (Sham, OVX-PBS, OVX-CST6, OVX-ZA) L3-L5 vertebrae protein lysate from each sample in the group was pooled. For pooled samples triplicate analysis was performed.

Figure 6: RNA-seq analysis of tibia from OVX-mouse model reveals potential different pathways for CST6 and ZA treatment. (**A**) Experimental workflow for RNA-seq experiment on tibia isolated from OVX mice. (**B**) 175 unique differentially expressed genes were found for OVX-CST6 treated tibia compared to the 12 differentially expressed genes for OVX-ZA treated tibia. (**C**) The top 10 genes with largest fold increase in the tibia following rmCst6 treatment of OVX mice are listed in a heat map and sorted by LS Mean. Of interest *Slco1a4*, an organic anion transporter that may be involved in bringing estrogen into the cell had the largest fold increase (log2 fold = 3.60). (**D**) The top 10 genes with the greatest fold change (increase or decrease) following ZA treatment of OVX tibia are listed in a heat map sorted by LS Mean. (**E-F**) Basal tissue and cell level gene expression of *Slco1a4* determined by PCR. (**G**) RNA-seq results for tibia were confirmed using real-time PCR on RNA isolated from L3-L5 vertebrae (n = 7). (**H-J**) Slco1a4 mRNA levels increases for both pre-osteoclastic Raw 264.7 cells treated with RANKL (20 ng/ml) as well as for pre-osteoblastic ST2 cells (+/- 1 mM A2P) (n = 3). Only the increase for Raw 264.7 cells was considered significant. Data represented as mean +/- SD analyzed by one-way ANOVA with Tukey's multiple-comparisons. Denoted markings are considered significant *$P < 0.05$, **$P < 0.01$, ***$P < 0.001$.

Figure 7: ERα expression in bone tissue and cells and intracellular total estrogen levels in osteoclast precursors are increased following treatment with rmCST6. (**A**) ERα protein levels are decreased in L3-L5 vertebrae of OVX mice and expression is brought back to sham surgery levels only by rmCst6 treatment (N = 6). Amido black staining was used as a loading

control. (**B**) Raw cells treated with either 1 μM ZA or 100 ng/ml of rmCST6 for 48 hr. had increased mRNA and protein levels of ERα when compared to control treated samples (N = 3). Protein level significance was analyzed using one-tailed t-test (**Table 4**). (**C**) Raw cells treated with 1 μM ZA or 100 ng/ml of rmCst6 for 48 hr. (20 ng/ml RANKL) had increased mRNA and protein levels of ERα when compared to control treated samples (N = 3). Protein level significance was analyzed using one-tailed t-test (**Table 5**). (**D**) Total intracellular estrogen levels (E1, E2, E3) for cultured osteoclast precursor cells isolated from mouse femur was increased for only 100 ng/ml rmCst6 treatment. Estrogen concentration was normalized to total protein lysate concentration. Graph is the result of triplicate experiments (N = 9). Three ELISA plates were scaled to each other by dividing estrogen concentration (pg/μg) for each sample by average estrogen concentration of control treatment for said plate, then multiplying by the average estrogen concentration for all samples across three plates. (**E**) Immunohistology staining of Raw 264.7 cells incubated for 24 hr. treated with PBS control solution or 100 ng/ml rmCST6. Cells treated with rmCst6 showed increased expression of ERα, whose transcription known to be upregulated by estrogen, and decreased expression of PPARγ, whose transcription is known to be downregulated by estrogen. (**F**) Immunohistology staining of Raw 264.7 cells incubated for 7 days treated with PBS control solution or 100 ng/ml rmCst6 (20 ng/ml RANKL). Cells treated with rmCst6 showed increased expression of ERα and decreased expression of PPARγ. (**G**) Estrogen influx is increased in Raw 264.7 cells by 24 hr. rmCst6 treatment. Raw 264.7 cells were plated onto tissue culture treated slides (Lab-Tek Chamber Slide System, 177437) at a concentration of 2.5 x 10^5 cells/ml and treated with PBS (left panel) or 100 ng/ml rmCst6 (right panel) and 1 pm Estradiol glow (E2 Glow, Jena Bioscience, PR-958S) for 24 hr. After 24 hr. media was aspirated and cells were fixed with cold 4% Paraformaldehyde for 20 min and rinsed with PBS. Following this, cells were covered with DAPI-Fluoromount-G and observed using a Nikon Eclipse T/2 epifluorescent microscope. DAPI ex wavelength: 350 nm, em wavelength: 470 nm; E2 Glow ex wavelength: 467 nm, em wavelength: 618 nm. Data represented as mean +/- SD analyzed by one-way ANOVA with Tukey's multiple-comparisons. Denoted markings are considered significant $*P < 0.05$, $**P < 0.01$, $***P < 0.001$.

Figure 1

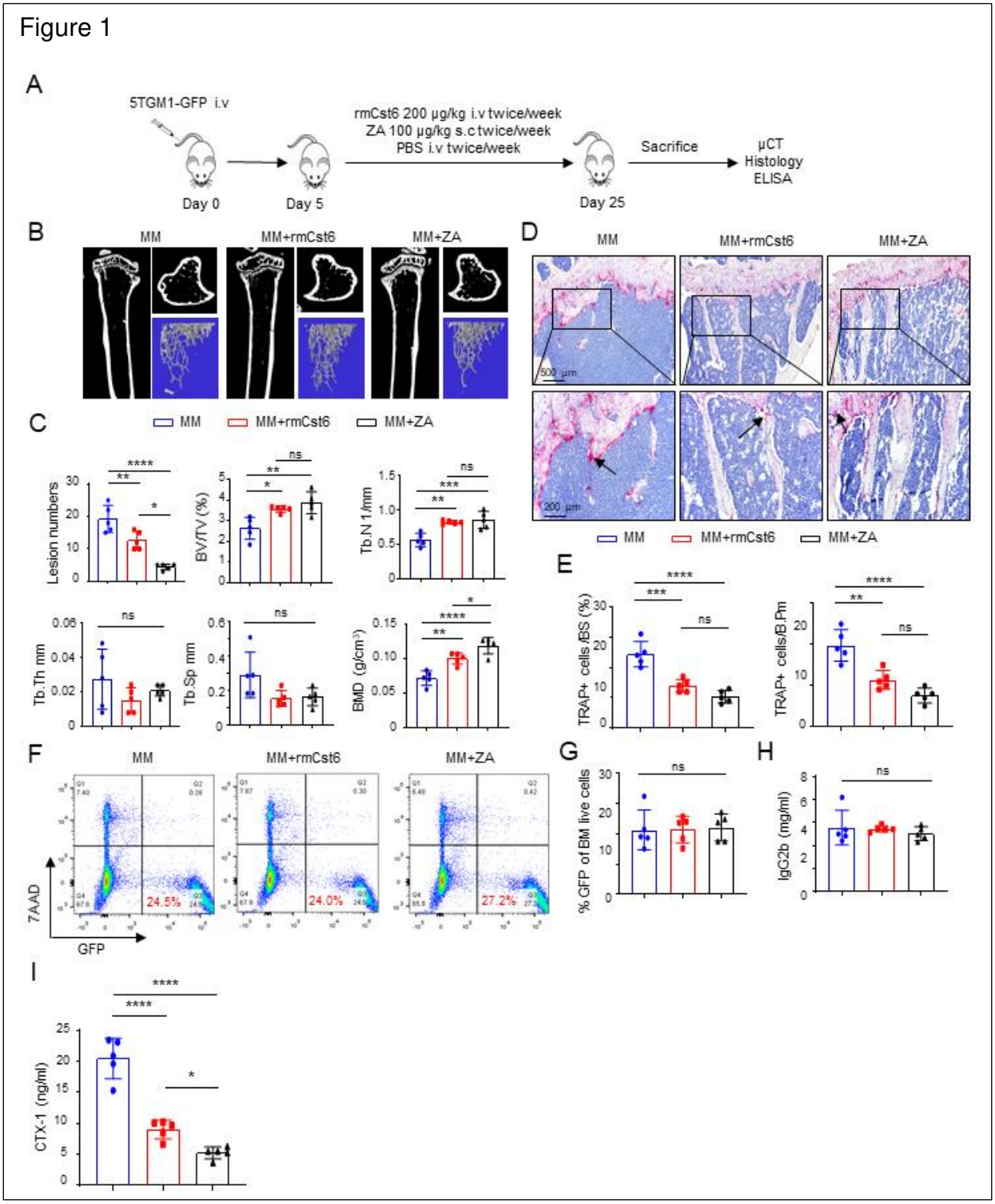
A
5TGM1-GFP i.v
Day 0
Day 5
rmCst6 200 μg/kg i.v twice/week
ZA 100 μg/kg s.c twice/week
PBS i.v twice/week
Day 25
Sacrifice
μCT
Histology
ELISA
B
MM
MM+rmCst6
MM+ZA
C
MM
MM+rmCst6
MM+ZA
Lesion numbers
BV/TV (%)
Tb.N 1/mm
Tb.Th mm
Tb.Sp mm
BMD (g/cm³)
D
MM
MM+rmCst6
MM+ZA
500 μm
200 μm
MM
MM+rmCst6
MM+ZA
E
TRAP+ cells/BS (%)
TRAP+ cells/B.Pm
F
MM
MM+rmCst6
MM+ZA
7AAD
GFP
24.5%
24.0%
27.2%
G
% GFP of BM live cells
H
IgG2b (mg/ml)
I
CTX-1 (ng/ml)

Figure 2

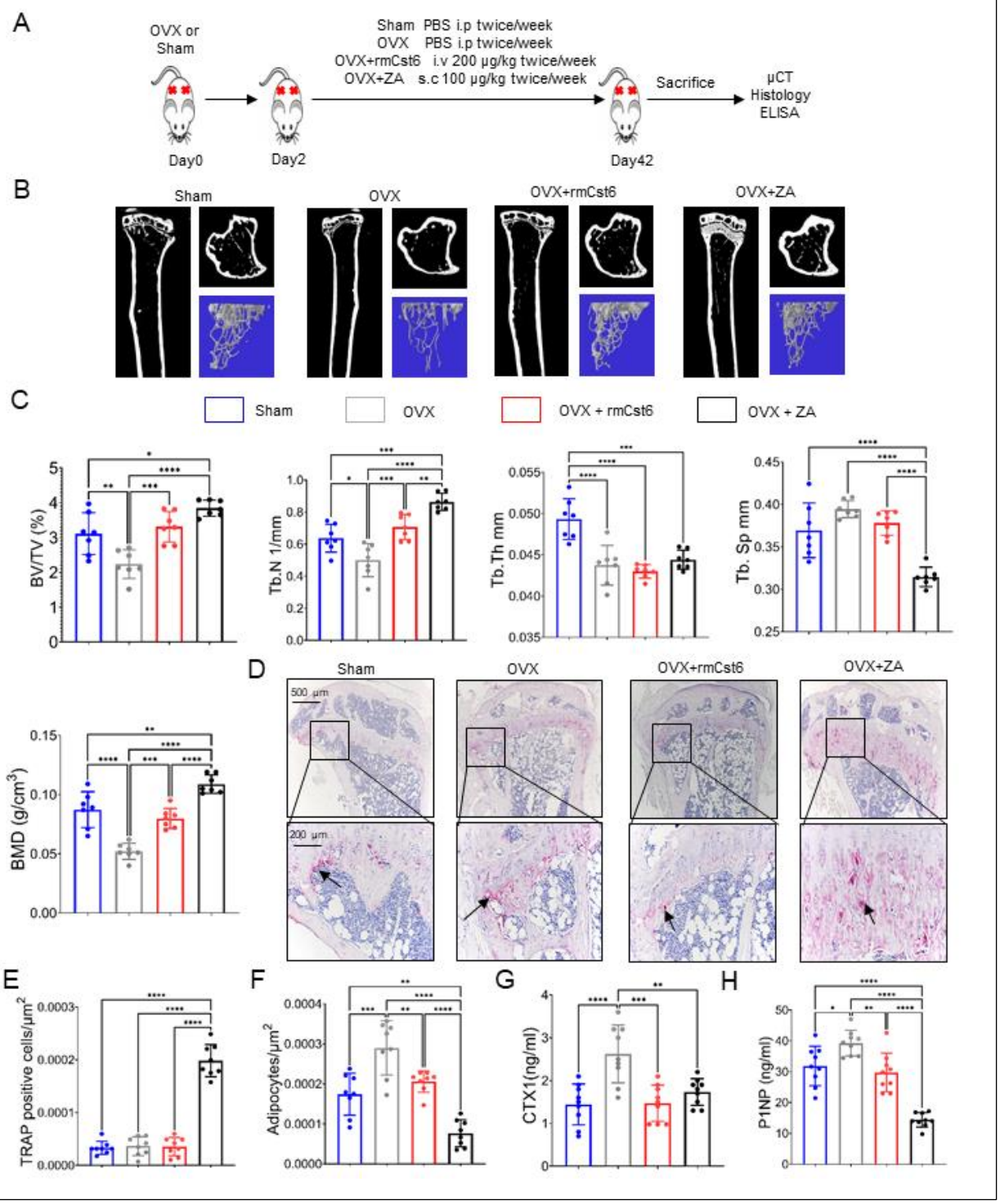
A
OVX or Sham
Sham PBS i.p twice/week
OVX PBS i.p twice/week
OVX+rmCst6 i.v 200 μg/kg twice/week
OVX+ZA s.c 100 μg/kg twice/week
Sacrifice
μCT
Histology
ELISA
Day0
Day2
Day42
B
Sham
OVX
OVX+rmCst6
OVX+ZA
C
Sham
OVX
OVX + rmCst6
OVX + ZA
BV/TV (%)
Tb.N 1/mm
Tb.Th mm
Tb. Sp mm
BMD (g/cm3)
D
Sham
OVX
OVX+rmCst6
OVX+ZA
500 μm
200 μm
E
TRAP positive cells/μm2
F
Adipocytes/μm2
G
CTX1(ng/ml)
H
P1NP (ng/ml)

958

Figure 3

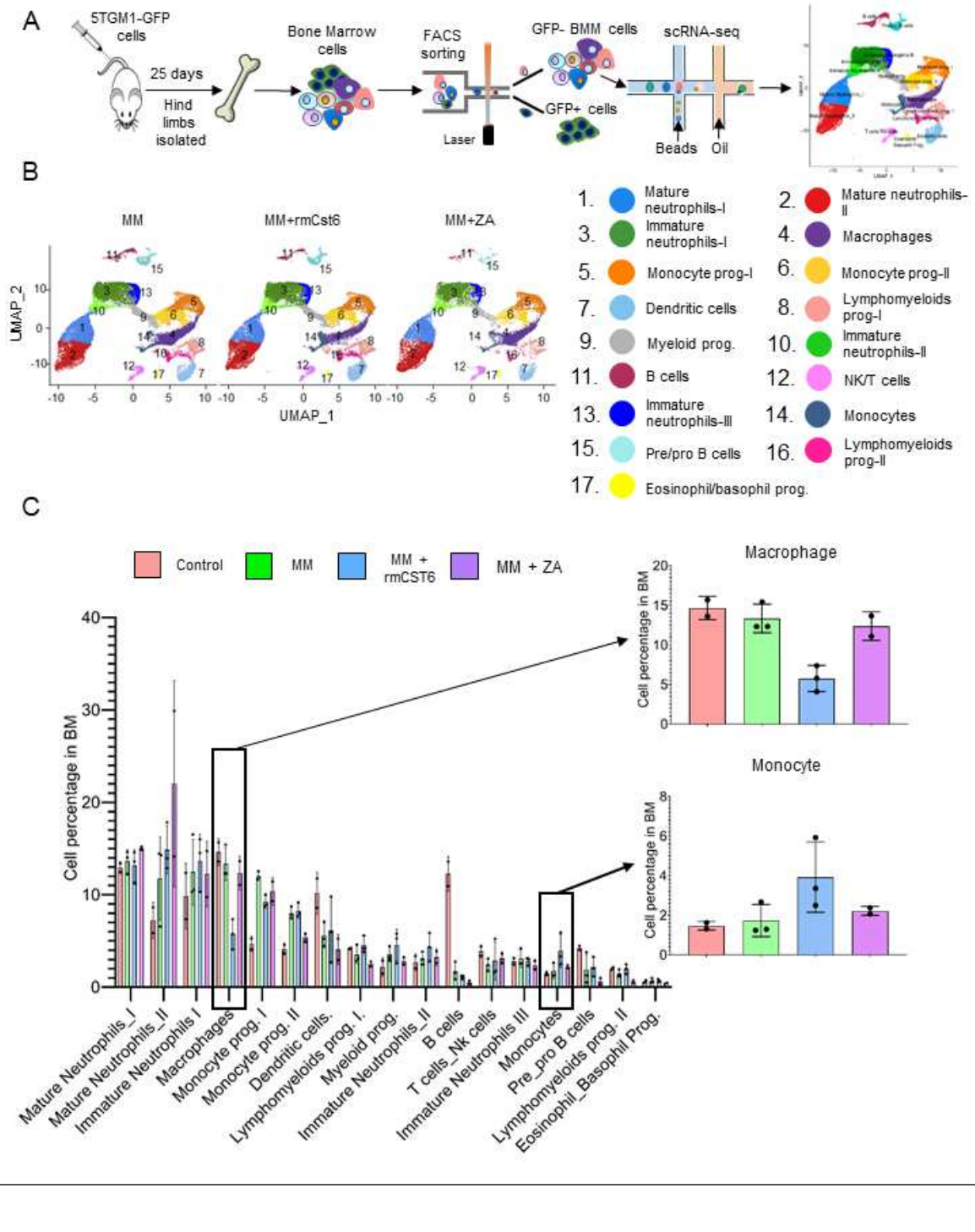
A
5TGM1-GFP cells
25 days
Hind limbs isolated
Bone Marrow cells
FACS sorting
Laser
GFP- BMM cells
GFP+ cells
scRNA-seq
Beads
Oil
B
MM
MM+rmCst6
MM+ZA
UMAP_2
UMAP_1
1. Mature neutrophils-I
2. Mature neutrophils-II
3. Immature neutrophils-I
4. Macrophages
5. Monocyte prog-I
6. Monocyte prog-II
7. Dendritic cells
8. Lymphomyeloids prog-I
9. Myeloid prog.
10. Immature neutrophils-II
11. B cells
12. NK/T cells
13. Immature neutrophils-III
14. Monocytes
15. Pre/pro B cells
16. Lymphomyeloids prog-II
17. Eosinophil/basophil prog.
C
Control
MM
MM + rmCST6
MM + ZA
Cell percentage in BM
Macrophage
Monocyte
Mature Neutrophils_I
Mature Neutrophils_II
Immature Neutrophils I
Macrophages
Monocyte prog. I
Monocyte prog. II
Dendritic cells.
Lymphomyeloids prog. I.
Myeloid prog.
Immature Neutrophils_II
B cells
T cells_Nk cells
Immature Neutrophils III
Monocytes
Pre_pro B cells
Lymphomyeloids prog. II
Eosinophil_Basophil Prog.

959

Figure 4

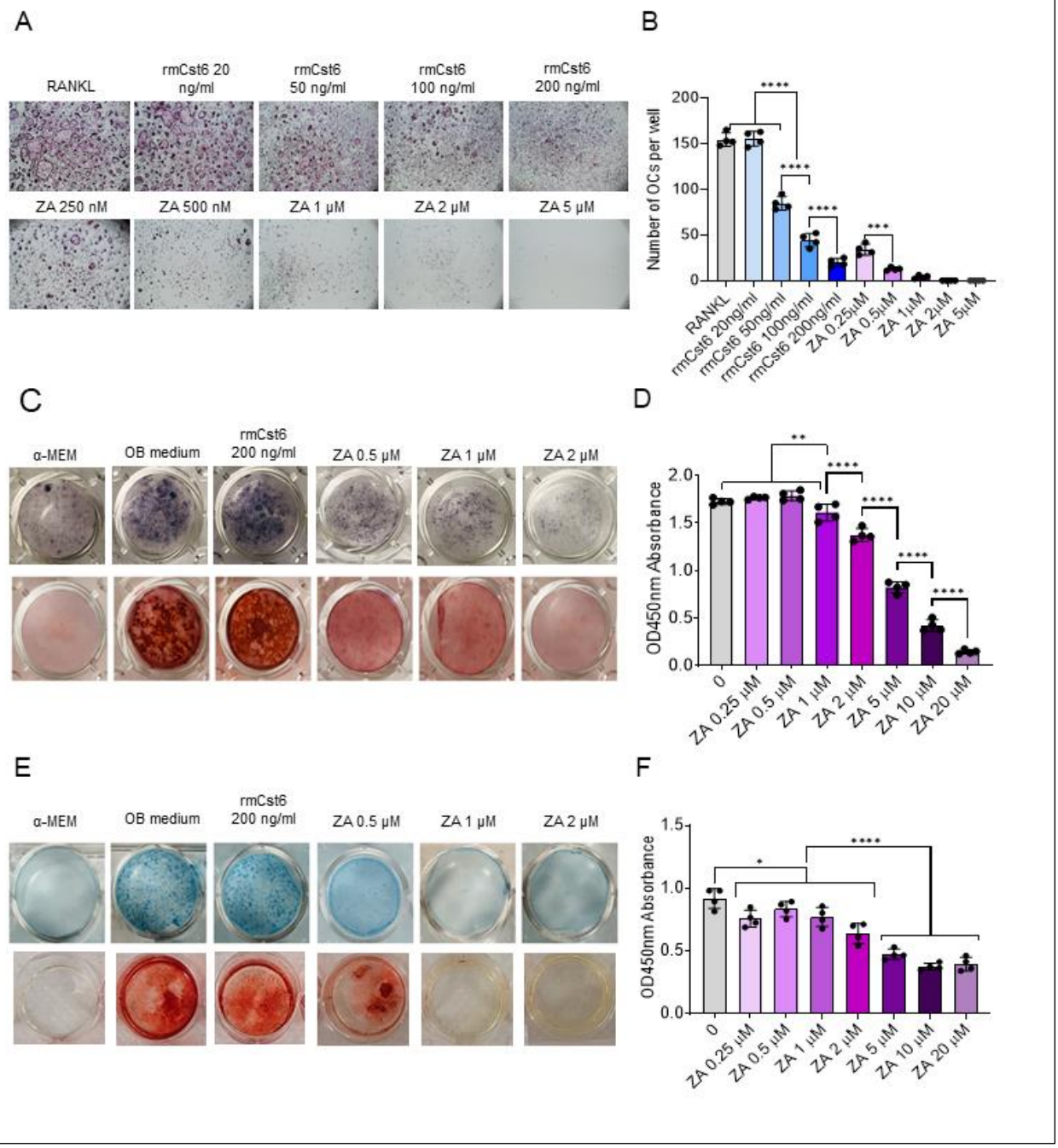

960

961

Figure 5

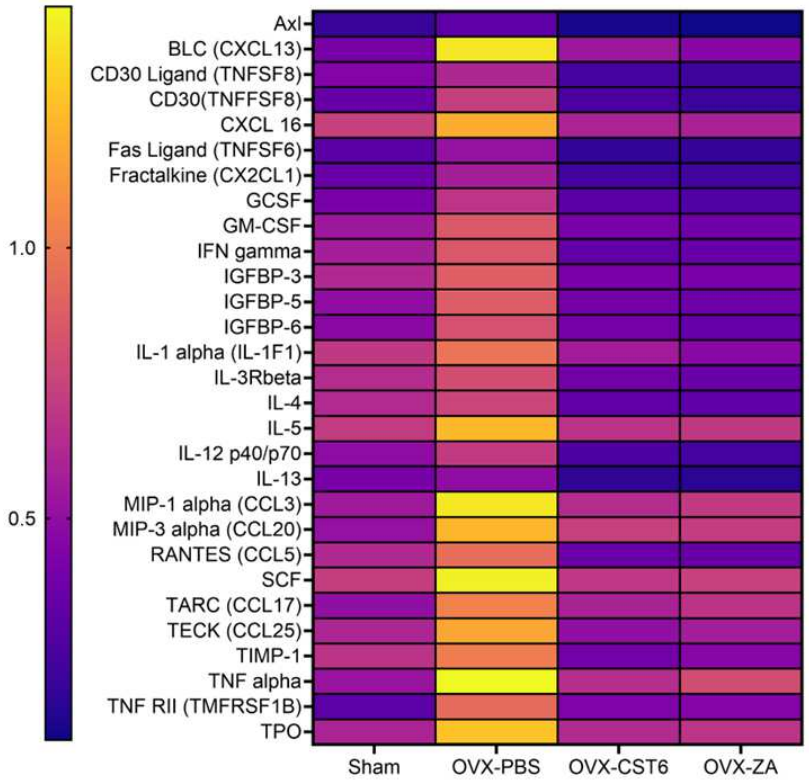

	Sham-PBS			OVX-PBS		OVX-rmCST6				OVX-ZA			
			2-way ANOVA P Value					2-way ANOVA P Value				2-way ANOVA P Value	
	AVER	STDEV	vs OVX	AVER	STDEV	AVER	STDEV	vs Sham	vs OVX	AVER	STDEV	vs Sham	vs OVX
Axl	0.2	0.2	0.8	0.3	0.1	0.1	0.06	0.9	0.4	0.09	0.05	0.9	0.5
BLC (CXCL13)	0.4	0.1	<0.0001	1.4	0.2	0.5	0.1	1.0	<0.0001	0.5	0.03	0.8	<0.0001
CD30 Ligand (TNFSF8)	0.4	0.03	0.6	0.6	0.03	0.2	0.04	0.4	0.04	0.2	0.03	0.5	0.07
CD30 (TNFFSF8)	0.3	0.06	0.06	0.7	0.2	0.3	0.02	0.8	0.006	0.2	0.02	0.9	0.01
CXCL 16	0.7	0.3	0.02	1.2	0.4	0.6	0.2	0.7	0.001	0.6	0.08	0.8	0.001
Fas Ligand (TNFSF6)	0.3	0.3	0.4	0.5	0.3	0.2	0.02	0.8	0.1	0.2	0.05	0.8	0.1
Fractalkine (CX2CL1)	0.4	0.2	0.4	0.6	0.3	0.2	0.03	0.8	0.09	0.2	0.04	0.8	0.1
GCSF	0.4	0.2	0.3	0.7	0.2	0.3	0.06	0.8	0.04	0.3	0.04	0.9	0.07
GM-CSF	0.5	0.2	0.2	0.9	0.1	0.4	0.08	0.6	0.01	0.4	0.03	0.8	0.02
IFN gamma	0.6	0.2	0.3	0.8	0.2	0.3	0.04	0.4	0.01	0.4	0.04	0.4	0.008
IGFBP-3	0.6	0.3	0.3	0.9	0.3	0.4	0.03	0.4	0.01	0.4	0.06	0.4	0.01
IGFBP-5	0.5	0.1	0.07	0.9	0.1	0.4	0.03	0.8	0.008	0.4	0.05	0.9	0.01
IGFBP-6	0.5	0.2	0.1	0.8	0.2	0.4	0.04	0.8	0.01	0.3	0.04	0.9	0.04
IL-1 alpha (IL-1F1)	0.7	0.3	0.3	1.0	0.4	0.6	0.1	0.4	0.009	0.5	0.03	0.7	0.04
IL-3Rbeta	0.6	0.1	0.7	0.8	0.1	0.4	0.1	0.2	0.02	0.4	0.06	0.3	0.04
IL-4	0.6	0.3	0.8	0.8	0.2	0.3	0.08	0.2	0.02	0.3	0.05	0.2	0.03
IL-5	0.7	0.1	0.006	1.2	0.1	0.7	0.07	1.0	0.004	0.7	0.06	1.0	0.003
IL-12 p40/p70	0.5	0.2	0.4	0.7	0.1	0.3	0.05	0.3	0.01	0.2	0.005	0.4	0.02
IL-13	0.4	0.07	0.9	0.5	0.07	0.2	0.02	0.3	0.1	0.2	0.04	0.4	0.1
MIP-1 alpha (CCL3)	0.6	0.3	<0.0001	1.4	0.8	0.6	0.06	0.7	0.0002	0.7	0.1	0.9	<0.0001
MIP-3 alpha (CCL20)	0.5	0.1	<0.0001	1.2	0.3	0.7	0.08	0.5	0.007	0.7	0.1	0.4	0.0103
RANTES (CCL5)	0.6	0.2	0.1	0.9	0.2	0.4	0.2	0.3	0.001	0.4	0.1	0.3	0.002
SCF	0.7	0.2	0.0001	1.4	0.04	0.7	0.1	1.0	0.0002	0.7	0.1	1.0	<0.0001
TARC (CCL17)	0.5	0.2	0.006	1.0	0.3	0.6	0.1	0.6	0.1	0.7	0.2	0.9	0.03
TECK (CCL25)	0.6	0.4	0.003	1.2	0.3	0.5	0.05	1.0	0.001	0.6	0.2	0.9	0.0003
TIMP-1	0.7	0.1	0.1	1.0	0.07	0.4	0.03	0.4	0.003	0.5	0.1	0.2	0.0007
TNF alpha	0.5	0.1	<0.0001	1.4	0.5	0.7	0.05	0.3	0.0005	0.8	0.05	0.8	<0.0001
TNF RII (TMFRSF1B)	0.3	0.1	0.0007	0.9	0.6	0.4	0.06	0.7	0.01	0.5	0.02	0.8	0.008
TPO	0.6	0.3	0.0003	1.3	0.3	0.6	0.02	0.9	0.001	0.7	0.07	1.0	0.0006

Figure 6

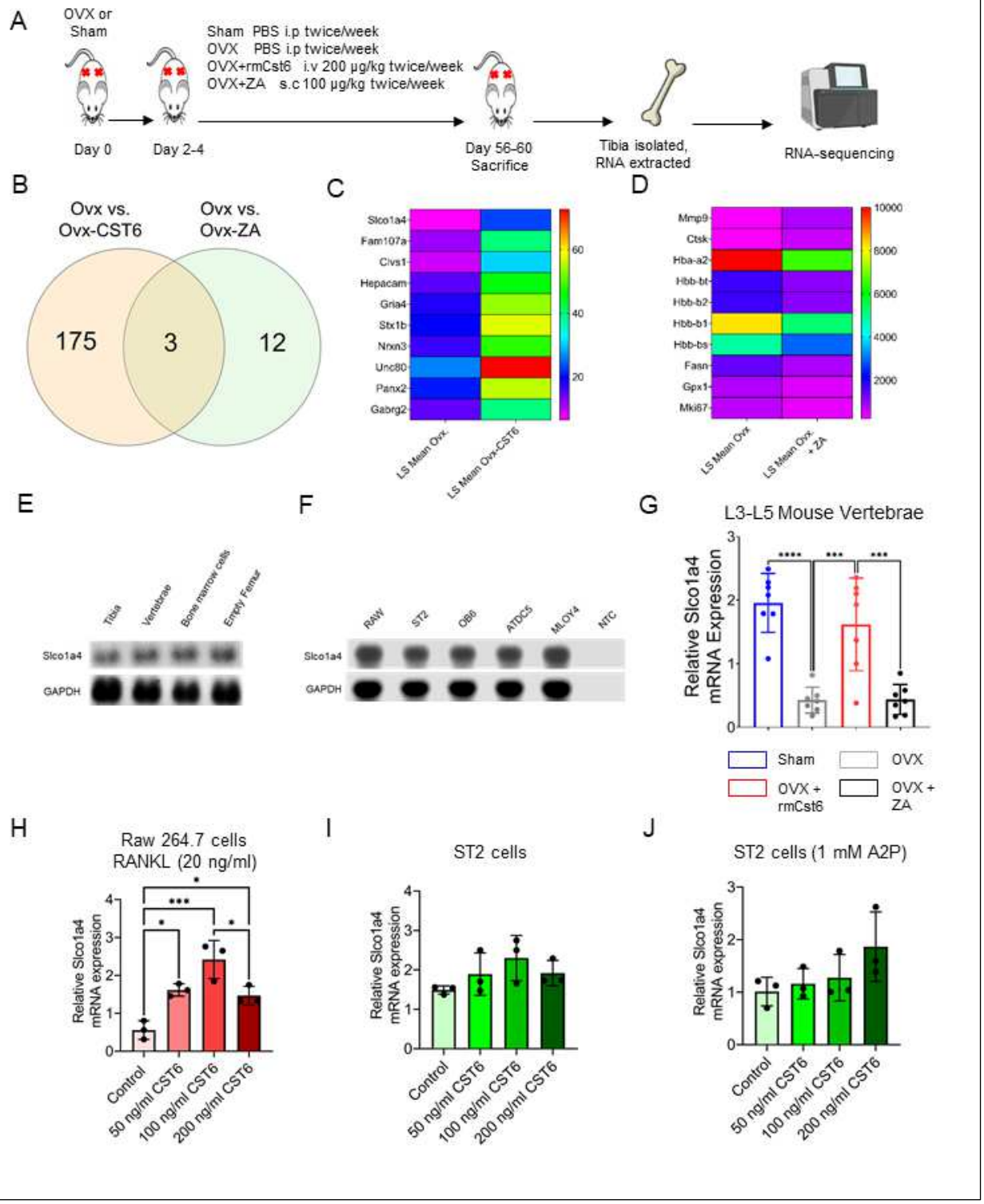

963

964

Figure 7

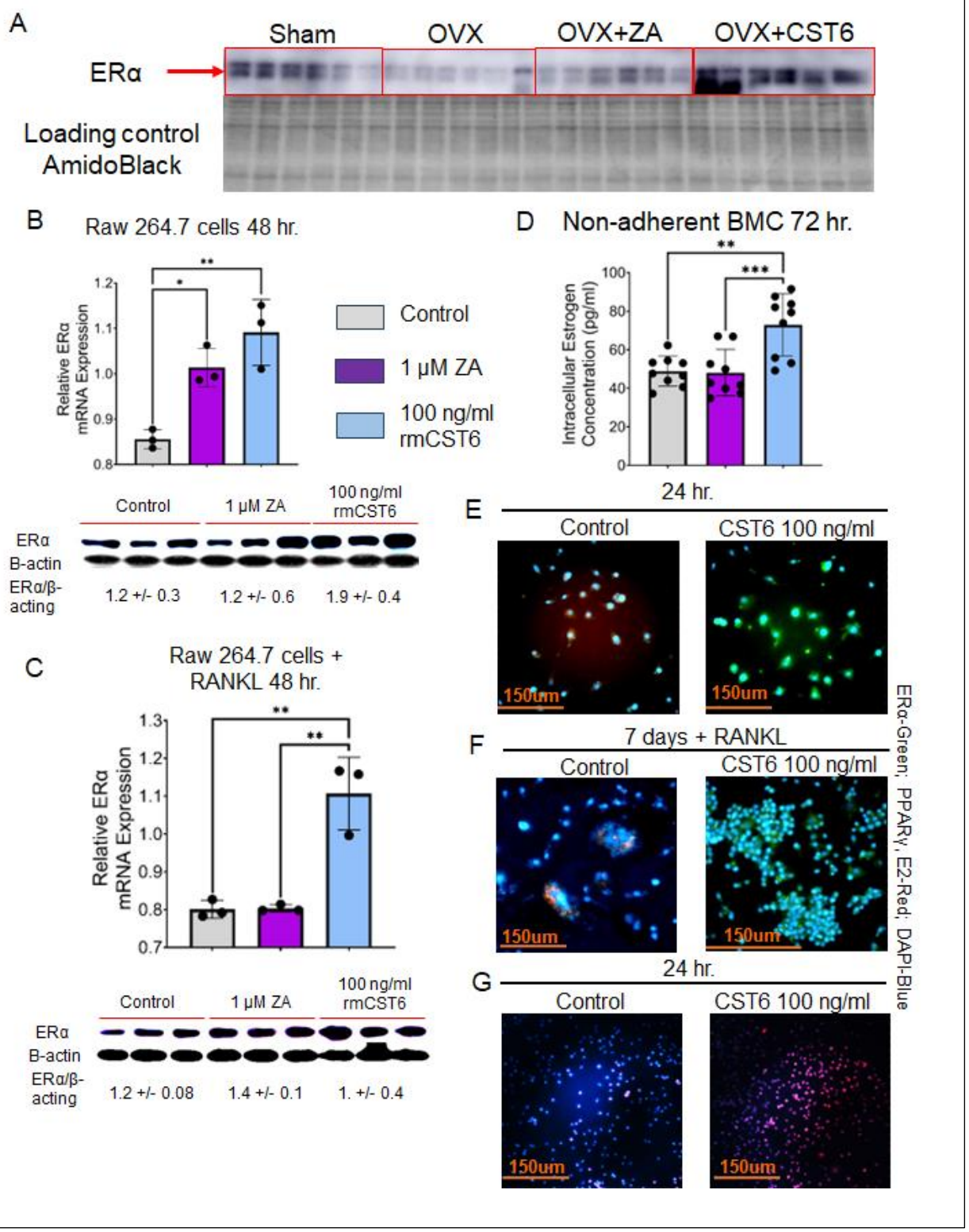
A
Sham
OVX
OVX+ZA
OVX+CST6
ERα
Loading control
AmidoBlack
B
Raw 264.7 cells 48 hr.
Relative ERα mRNA Expression
Control
1 μM ZA
100 ng/ml rmCST6
Control
1 μM ZA
100 ng/ml rmCST6
ERα
B-actin
ERα/β-acting
1.2 +/- 0.3
1.2 +/- 0.6
1.9 +/- 0.4
C
Raw 264.7 cells + RANKL 48 hr.
Relative ERα mRNA Expression
Control
1 μM ZA
100 ng/ml rmCST6
ERα
B-actin
ERα/β-acting
1.2 +/- 0.08
1.4 +/- 0.1
1. +/- 0.4
D
Non-adherent BMC 72 hr.
Intracellular Estrogen Concentration (pg/ml)
E
24 hr.
Control
CST6 100 ng/ml
150um
F
7 days + RANKL
Control
CST6 100 ng/ml
150um
G
24 hr.
Control
CST6 100 ng/ml
150um
ERα-Green; PPARγ, E2-Red; DAPI-Blue

965

966 **Supplementary Figures**

Supplementary Figure 1

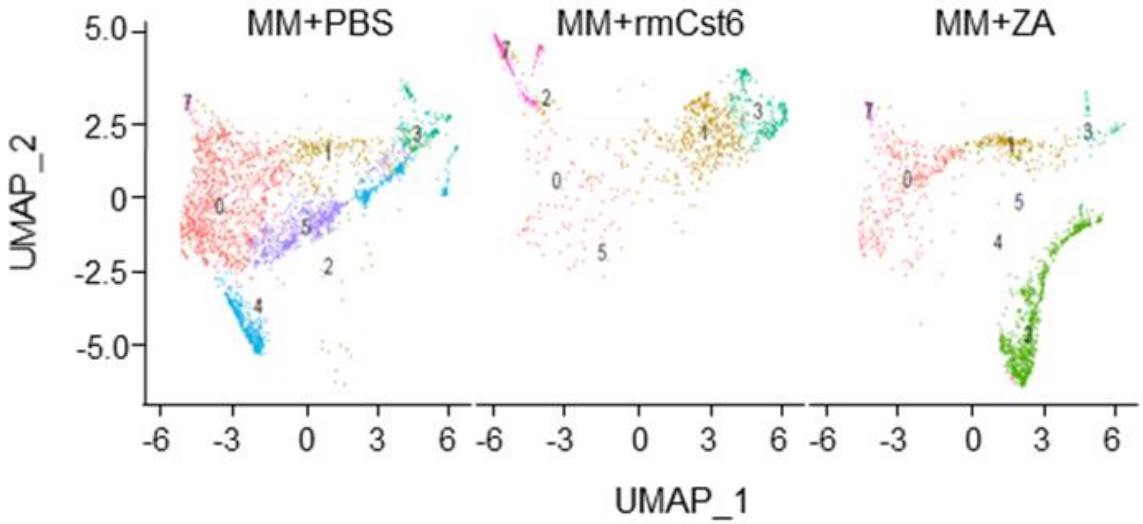

Supplementary Figure 1: UMAP plot of bone marrow macrophages following MM mouse model treatment with either PBS control solution (n = 3), rmCst6 (n = 3), or ZA (n = 2). Compared to control treated mice rmCst6 treatment decreased the amount of M0, M4 and M5 macrophages present in the bone marrow while increasing the percentage of M7 macrophage present. Following ZA treatment; M0, M3, M4 and M5 macrophage sub-clusters are decreased while the M2 macrophage sub-cluster is increased. However, M0 macrophages, which are considered osteoclast precursors are not decreased to the extent of rmCst6 treatment.

967

968